CHALMERS
UNIVERSITY OF TECHNOLOGY

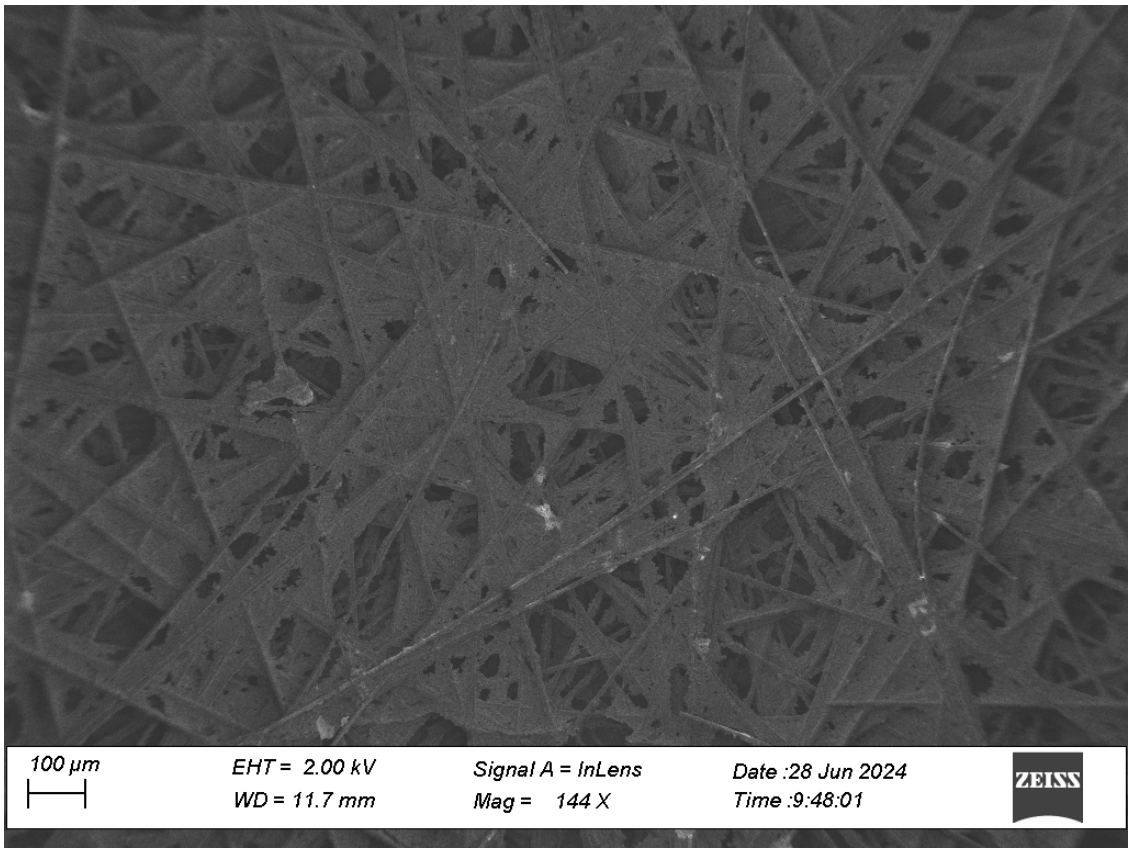

Comprehensive Analysis of PTFE distribution in Gas Diffusion Layers Using Advanced Ex-situ and In-situ Characterization Techniques

Master's Thesis in Chemistry and chemical Engineering

SIVA BALAGANESH RAVI SANKAR

DEPARTMENT OF APPLIED CHEMISTRY

CHALMERS UNIVERSITY OF TECHNOLOGY
Gothenburg, Sweden 2024
www.chalmers.se

Master Thesis report 2024

Comprehensive Analysis of PTFE distribution in Gas Diffusion Layers Using Advanced Ex-situ and In-situ Characterization Techniques

SIVA BALAGANESH RAVI SANKAR

CHALMERS
UNIVERSITY OF TECHNOLOGY

Department of Applied Chemistry
Chalmers University of Technology
Gothenburg, Sweden 2024

Comprehensive Analysis of PTFE distribution in Gas Diffusion Layers Using Advanced Ex-situ and In-situ Characterization Techniques
SIVA BALAGANESH RAVI SANKAR

Supervisor: Marcus Ringström, Development Engineer - Powercell Group
Co-Supervisor: Dylan Schulz, Doctoral Student, Chemistry and Chemical Engineering - Chalmers University of Technology
Examiner: Anna Martinelli, Professor Chemistry and Chemical Engineering - Chalmers University of Technology

Master Thesis report 2024
Department of Applied Chemistry
Chalmers University of Technology
SE-412 96 Gothenburg
Sweden
Telephone +46 31 772 1000

Cover: Fuel cell Technology

Typeset in LaTeX
Gothenburg, Sweden 2024

Comprehensive Analysis of PTFE distribution in Gas Diffusion Layers Using Advanced Ex-situ and In-situ Characterization Techniques
SIVA BALAGANESH RAVI SANKAR
Department of Applied Chemistry
Chalmers University of Technology

Abstract

The performance and longevity of Proton Exchange Membrane Fuel Cells (PEMFCs) are critically dependent on the properties of the gas diffusion layer (GDL). This study investigates the hydrophobic treatment using the dip coating method on two types of GDLs, namely dry-laid and wet-laid, using polytetrafluoroethylene (PTFE) at target concentrations of 5 wt%, 20 wt%, and 50 wt%. The distribution of PTFE across the thickness and surface of the GDLs is characterized to understand its impact on water management and gas transport properties. The effectiveness of the hydrophobic treatment is evaluated both ex-situ via contact angle measurements and in-situ by limiting the current density to assess oxygen transport resistance. Additionally, advanced characterization techniques, including Scanning Electron Microscopy (SEM), Energy Dispersive X-ray Spectroscopy (EDX), and Raman Spectroscopy, are employed to provide a detailed analysis of PTFE distribution, correlating these findings with the GDL's performance in operating PEMFCs.

Key findings reveal that while increased PTFE concentration improved hydrophobicity and water management, excessive PTFE loading led to pore blockage, negatively impacting oxygen transport resistance. The wet-laid GDL demonstrated more uniform PTFE distribution and higher transport resistance compared to the dry-laid GDL. These insights emphasize the importance of balancing PTFE concentration to optimize both water management and gas diffusion in PEMFCs.

Keywords: Gas diffusion layer, Proton exchange membrane fuel cell, PTFE, Dip-coating method, Limiting current Density.

Acknowledgements

I would like to express my sincere gratitude to everyone who supported and guided me throughout the course of this thesis.

Firstly, I extend my heartfelt thanks to **Marcus Ringström** at PowerCell for his invaluable supervision, providing consistent support, guidance, and insight, from experiment planning to interpreting the results. I am also deeply thankful to **Kalle Genheden** and **Victor Shokhen** for their essential help in facilitating the in-situ measurements, which were a pivotal part of this research. Additionally, I appreciate **Gert Göransson** and **Marika Männikkö** for their assistance in helping me acclimate to the lab environment and ensuring all safety protocols were followed during the initial stages of my work.

At Chalmers, I owe special thanks to my examiner, **Anna Martinelli**, who provided crucial support with the Raman spectroscopy, and to my co-supervisor, **Dylan Schulz**, who ensured I was able to record and analyze results across all characterization techniques. I am particularly grateful to **Romain Bordes**, **Stefan Gustafsson**, and **Suichi Haraguchi**, whose assistance in conducting TGA, SEM & EDX, and contact angle measurements proved vital to the success of this thesis. Special thanks go to **Andreas Schaefer** for his guidance with the calcination oven during the heat treatment of the GDLs, and to **Mats Hulander** for ensuring I was well-versed in safety protocols in the chemistry labs.

Finally, I extend my deepest appreciation to all of the individuals mentioned above, without whose generous contributions and support, this thesis would not have reached its full potential. Your help has been invaluable to me, and for that, I am truly thankful.

SIVA BALAGANESH RAVI SANKAR, Gothenburg, September 2024

List of Acronyms

Below is the list of acronyms that have been used throughout this thesis:

PEMFC	Proton Exchange Membrane Fuel Cell
GDL	Gas Diffusion Layer
F-H23	Freudenberg H23
MPL	Micro Porous Layer
CL	Catalyst Layer
Rt	Transport resistance
SEM	Scanning Electron Microscopy
EDX	Energy Dispersive X-Ray Analysis
ilim	Limiting Current Density

Contents

List of Figures

List of Tables

1

Introduction

In the quest for sustainable and clean energy solutions, fuel cells have emerged as a promising technology for efficient energy conversion. Various types of fuel cells exist, each with its own set of characteristics and applications. Alkaline Fuel Cells (AFCs), for example, are known for their high efficiency and were used in the Apollo space missions, but they are limited by their sensitivity to carbon dioxide. Phosphoric Acid Fuel Cells (PAFCs) operate at higher temperatures and are suitable for stationary power generation, but they have relatively lower power density. Molten Carbonate Fuel Cells (MCFCs) and Solid Oxide Fuel Cells (SOFCs) operate at very high temperatures and are typically used for large-scale power generation due to their high efficiency and ability to use various fuels, but their thermal management and durability pose challenges [5].

Among these, Polymer Electrolyte Membrane Fuel Cells (PEMFCs) stand out for their versatility, low operating temperature, and fast start-up times, making them particularly suitable for applications such as portable electronics, transportation, and stationary power generation. PEMFCs offer a highly efficient and environmentally friendly means of converting chemical energy directly into electrical energy. Their high energy efficiency, rapid start-up capabilities, and ability to operate at relatively low temperatures (typically 60-80°C) have driven significant interest in their development, particularly in the transportation and portable power sectors.[6]

At the heart of a PEMFC lies the **Membrane Electrode Assembly (MEA)**, a multi-layered structure where the core electrochemical reactions take place [7]. Among the various components of the MEA, the **Gas Diffusion Layer (GDL)** plays a pivotal role in ensuring the efficient operation of the fuel cell. The GDL serves as the interface between the catalyst layer and the bipolar plates, facilitating the transport of reactant gases (hydrogen and oxygen) to the catalyst sites while simultaneously managing the water produced during the electrochemical reactions. Effective water management is crucial in PEMFCs; excessive water can lead to flooding, blocking the pores of the GDL and preventing the diffusion of reactants, which in turn can severely hinder fuel cell performance. Conversely, inadequate water retention can cause the membrane to dry out, leading to increased resistance and reduced proton conductivity.

To address these challenges, the GDL is typically treated with a hydrophobic agent to balance water management and gas transport. **Polytetrafluoroethylene (PTFE)** [8]is the most commonly used hydrophobic treatment for GDLs due to its superior

hydrophobic properties, chemical stability, and thermal resistance. PTFE treatment enhances the GDL's ability to repel water, preventing flooding and ensuring the continuous supply of oxygen to the catalyst sites, which is essential for maintaining high fuel cell efficiency. However, the effectiveness of PTFE as a hydrophobic treatment is not solely dependent on its presence but critically on its distribution across the GDL. Uneven PTFE distribution can result in localized flooding or drying, both of which can negatively impact fuel cell performance.

This thesis focuses on the hydrophobic treatment of two distinct types of GDLs: **dry-laid** and **wet-laid**. The dry-laid GDLs, such as the **SGL 39AA**, are manufactured by distributing fibers in a dry state and bonding them using mechanical, thermal, or chemical methods. This process results in GDLs with highly uniform porosity and thickness, offering high mechanical strength and durability. In contrast, wet-laid GDLs, like the **Freudenberg H23**, are produced by suspending fibers in a liquid medium, typically water, followed by a drying process that forms a bonded fiber network. Wet-laid GDLs are generally more cost-effective and scalable for large-scale production but may exhibit greater variability in porosity and thickness, leading to differences in performance.

In this study, both types of GDLs are treated with varying concentrations of PTFE specifically, 5 wt%, 20 wt%, and 50 wt%—to investigate the optimal hydrophobic treatment for enhancing PEMFC performance. Advanced characterization techniques, including **Scanning Electron Microscopy (SEM)** and **Energy Dispersive X-ray Spectroscopy (EDX)**, are employed to analyze the distribution and dispersion of PTFE across the GDL surface and through its thickness. These techniques provide a detailed understanding of the microstructural changes induced by PTFE treatment and how these changes influence the GDL's ability to manage water and facilitate gas transport.

Another critical aspect of this research is the assessment of **oxygen transport resistance**, which is a key factor in determining the efficiency of PEMFCs. Oxygen transport resistance directly affects the availability of oxygen at the catalyst sites, and therefore the overall reaction rate and efficiency of the fuel cell. The **limiting current density method** is utilized in this study to quantify the oxygen transport resistance in the GDLs treated with different PTFE concentrations. This method provides insight into how PTFE concentration and GDL type impact oxygen diffusion and how these variables can be optimized to improve fuel cell performance[9][10].

2
Background

A comprehensive literature review was conducted to explore the key components and operational principles of Proton Exchange Membrane Fuel Cells (PEMFCs), with a specific focus on the Gas Diffusion Layer (GDL) and its role in fuel cell performance. The review delved into the fundamental processes governing PEMFC operation, the materials and structures of the Membrane Electrode Assembly (MEA), and the importance of optimizing GDL properties for efficient gas and water transport. By examining existing studies, various GDL manufacturing techniques and hydrophobic treatment methods, such as the application of polytetrafluoroethylene (PTFE), were identified as critical factors in enhancing fuel cell performance and durability. The following sections provide an in-depth discussion of the working principles, key components, and the significance of the GDL in achieving optimal performance in PEMFC systems.

2.0.1 Working Principle of PEMFC

A Proton Exchange Membrane Fuel Cell (PEMFC) operates at typical temperatures ranging from 60 to 120°C[11], converting chemical energy from hydrogen and oxygen directly into electrical energy through a series of electrochemical reactions. The process begins at the **anode**, where hydrogen gas (H_2) is introduced and splits into protons (H^+) and electrons (e^-) in the anode catalyst layer through the hydrogen oxidation reaction (HOR):[11]

$$2H_2 \rightarrow 4H^+ + 4e^-$$

The generated electrons are conducted away from the anode through the gas diffusion layer (GDL), flow field plate (FFP), and external circuit, creating an electric current that can be utilized to perform work. Simultaneously, the protons migrate through the proton-conductive polymer membrane to the cathode.
At the **cathode**, oxygen gas (O_2) is reduced in the cathode catalyst layer. The oxygen molecules combine with the incoming electrons from the external circuit and the protons that have migrated through the membrane, resulting in the production of water and the release of heat:

$$O_2 + 4e^- + 4H^+ \rightarrow 2H_2O$$

This reaction, known as the oxygen reduction reaction (ORR), occurs at the triple-phase boundary (TPB) within the cathode. The ORR is typically the rate-limiting step in PEMFCs due to its slower kinetics compared to the hydrogen oxidation reaction (HOR) at the anode, making it a critical focus in fuel cell development.

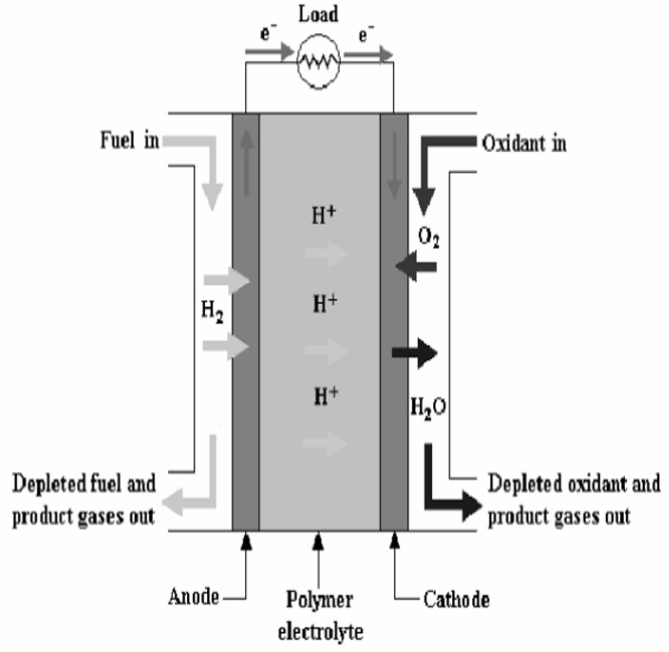

Figure 2.1: Working Principle of a PEMFC[1] image has been reproduced form the citation

The water produced at the cathode must be carefully managed to prevent excessive accumulation, which can lead to **flooding**. Flooding occurs when water fills the pores of the GDL, obstructing the pathways for gas transport and reducing the availability of reactants at the catalyst sites. To mitigate this issue, GDLs are often treated with hydrophobic agents like polytetrafluoroethylene (PTFE) to enhance their ability to repel water, ensuring that the pores remain open for efficient gas diffusion[2].

Polarization Curves and Losses:

The performance of a PEMFC is commonly characterized by its polarization curve, which plots the cell voltage against the current density. The curve typically consists of three regions, each dominated by different types of losses:

1. **Activation Losses:** These losses occur mainly at low current densities and are related to the activation energy required for the electrochemical reactions at the anode and cathode. The ORR at the cathode is particularly impacted due to its slower kinetics.
2. **Ohmic Losses:** These losses are due to resistance in the flow of electrons through the cell's components (such as the GDL, bipolar plates, and external circuit) and the resistance to proton flow through the electrolyte membrane. Ohmic losses increase linearly with current density.
3. **Mass Transport Losses:** At high current densities, the transport of reactants to the catalyst sites becomes limited. This limitation can cause a drop in cell voltage due to insufficient reactant supply or poor removal of product water, exacerbating issues such as flooding.

In a PEMFC, the simultaneous transport of water, gases, heat, and charge (protons and electrons) is critical to maintaining efficient operation. The management of these

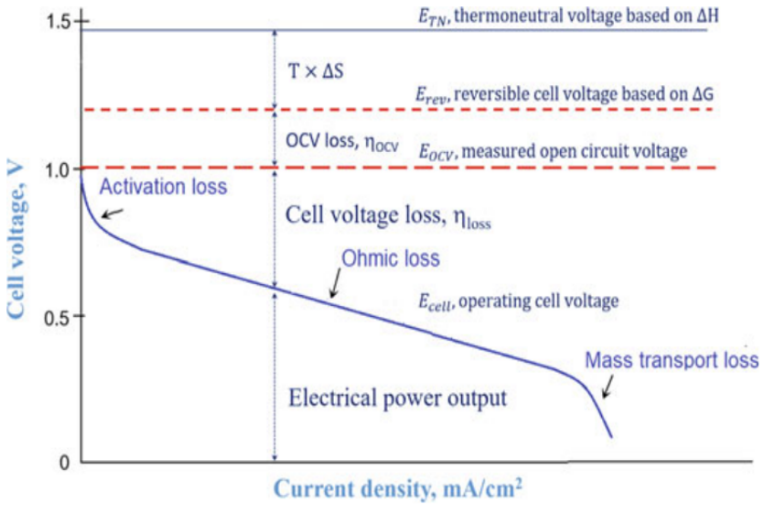

Figure 2.2: Polarisation curve representing the different loses in a PEMFC[2] image has been reproduced form the citation

transport processes within the membrane-electrode-assembly (MEA), especially the careful control of water to prevent flooding while maintaining adequate hydration of the membrane, is key to achieving high performance and durability in fuel cells.

2.0.2 Membrane Electrode Assembly (MEA)

The Membrane Electrode Assembly (MEA) is a critical component of a Proton Exchange Membrane Fuel Cell (PEMFC), where the key electrochemical reactions occur. The MEA is a sandwich-like structure composed of several layers that work together to convert chemical energy into electrical energy.
The **Gas Diffusion Layer (GDL)**, usually made of carbon fibers and a carbonaceous binder, typically 150 to 250 microns thick, is a crucial interface within the fuel cell, situated between the catalyst layer and the bipolar plate (BPP). While not the core of the Membrane Electrode Assembly (MEA), the GDL plays an essential role in ensuring that reactant gases (hydrogen and oxygen) are efficiently transported to the electrocatalyst sites and in facilitating the removal of water produced during electrochemical reactions. Effective management of water and gas transport within the GDL is critical for maintaining optimal fuel cell performance, as it interfaces with both the MEA and the BPPs to support the overall function of the fuel cell [2].
The **Microporous Layer (MPL)** is a thin layer coated on the GDL and is typically composed of carbon-based materials with a high surface area. The MPL is distinct from the GDL in terms of its function and composition. While the GDL primarily serves as a structural support and a macroporous medium for gas diffusion, the MPL has a finer pore structure and plays a more refined role in enhancing the overall performance, durability, and reliability of the fuel cell. It improves gas diffusion, water management, electrical conductivity, and mechanical stability by providing a controlled pathway for gases and liquids [12]. The smaller pores in the MPL allow for

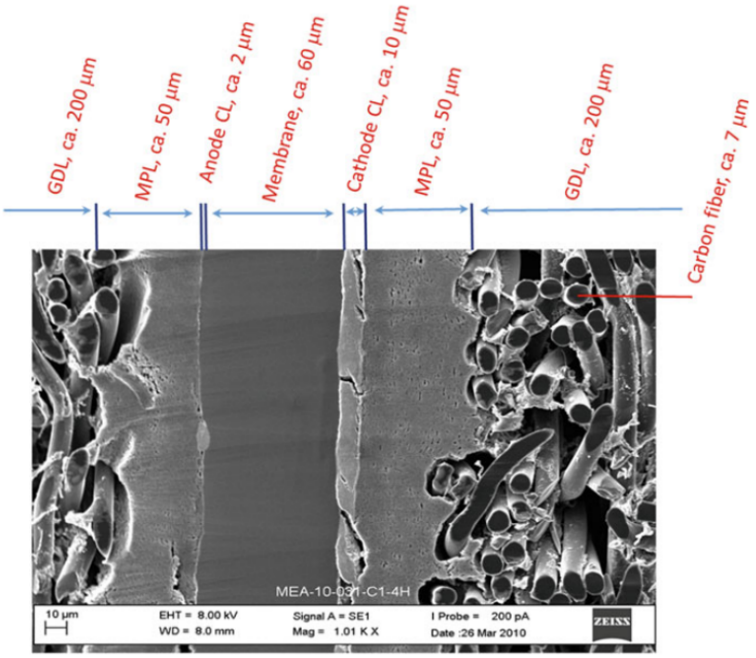

Figure 2.3: MEA assembly of a PEMFC[2] image has been reproduced form the citation

better water management by preventing liquid water from flooding the catalyst layer while also aiding in uniform gas distribution across the catalyst sites. In essence, the MPL acts as a bridge between the larger, more porous GDL and the catalyst layer, ensuring efficient transport of reactants and removal of products under varied operating conditions.

On top of the MPL is the **Catalyst Layer**, a thin coating typically consisting of platinum nanoparticles dispersed on a carbon support and mixed with a polymer binder. This layer is crucial for the electrochemical reactions that generate electricity in the fuel cell. The high surface area provided by the MPL increases the likelihood of reactant gases interacting with the catalyst, facilitating the splitting of hydrogen into protons and electrons.

The **Proton-Conductive Membrane** in the MEA, usually made of Nafion, allows protons generated at the anode to pass through to the cathode while blocking electrons, which travel through an external circuit to create electric current. Additionally, the membrane separates the hydrogen and oxygen reactants and withstands the harsh operating conditions of the fuel cell, such as high temperatures.

Bipolar Plates (BPs), also known as Flow Field Plates (FFPs), are multifunctional components of the MEA. They are responsible for evenly distributing the fuel gas and air across the MEA, conducting electrical current between cells in a fuel cell stack, and facilitating heat removal from the active area. Bipolar plates also prevent the leakage of gases and coolant, making them essential for the efficient and safe operation of the fuel cell.[2]

2.0.3 Gas Diffusion Layer (GDL)

The Gas Diffusion Layer (GDL) serves as the interface between the catalyst layer and the bipolar plate in a PEMFC. It provides a crucial pathway for reactants to reach the electrocatalyst sites and facilitates the removal of product water generated during the electrochemical reaction. Proper management of this water is essential to prevent flooding, which could block the reactants' access to the catalyst sites and severely degrade fuel cell performance.
The Gas Diffusion Layer (GDL) is primarily composed of carbon fibers that are often coated with a hydrophobic agent, such as polytetrafluoroethylene (PTFE). This hydrophobic coating helps maintain open pathways within the GDL by reducing the tendency of water droplets to adhere to the fibers, thereby managing water accumulation and facilitating efficient gas transport. Rather than creating micropores, the PTFE coating minimizes the surface tension between the carbon fibers and water, preventing the blockage of pores and ensuring that reactant gases can reach the catalyst sites. This balance between gas transport and water management is crucial for the optimal operation of the fuel cell. The GDL acts as a critical interface, aiding in the proper functioning of the overall fuel cell system.[4]

2.0.4 Types of Gas Diffusion Layers (GDLs)

Gas Diffusion Layers (GDLs) can be categorized into two main types based on their manufacturing processes: dry-laid and wet-laid[13]. Each type has unique characteristics that affect the performance and suitability of the GDL for different applications in PEMFCs. In this study, two types of GDLs were used: SGL 39AA, a dry-laid GDL, and Freudenberg H23, a wet-laid GDL.

2.0.4.1 Dry-Laid Gas Diffusion Layers (GDLs)

Dry-laid GDLs are produced by distributing fibers in a dry state and bonding them using mechanical, thermal, or chemical processes, often with the use of binders to enhance stability. This method results in GDLs with highly consistent porosity and thickness, which are essential for ensuring reliable performance in fuel cells. The controlled fiber distribution during the dry-laid process also contributes to the high mechanical strength and durability of these GDLs. Although this method is generally more expensive and complex compared to other manufacturing techniques, it offers significant advantages in terms of customization and material consistency, making dry-laid GDLs particularly suitable for high-performance PEM fuel cells.[13]

2.0.4.2 Wet-Laid Gas Diffusion Layers (GDLs)

Wet-laid GDLs are produced by first suspending fibers in a liquid medium, typically water, to create a slurry. This slurry is then deposited onto a moving screen or conveyor belt, where the liquid is removed through drying processes, resulting in a bonded fiber network. The wet-laid process can lead to variability in the porosity and thickness of the GDL due to the nature of slurry deposition and drying. However, wet-laid GDLs are generally more cost-effective and scalable, making them suitable

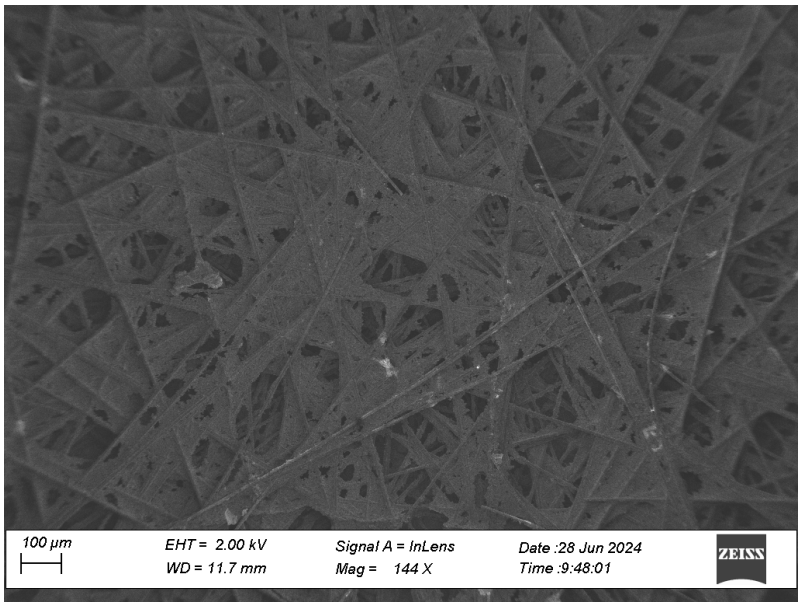

Figure 2.4: SEM image of Dry Laid SGL 39AA

for large-scale production. They are typically less mechanically robust compared to dry-laid GDLs but offer the advantage of being adaptable to various fiber types and blends. This method is particularly useful in applications where cost and scalability are prioritized over extreme uniformity and strength.[14]

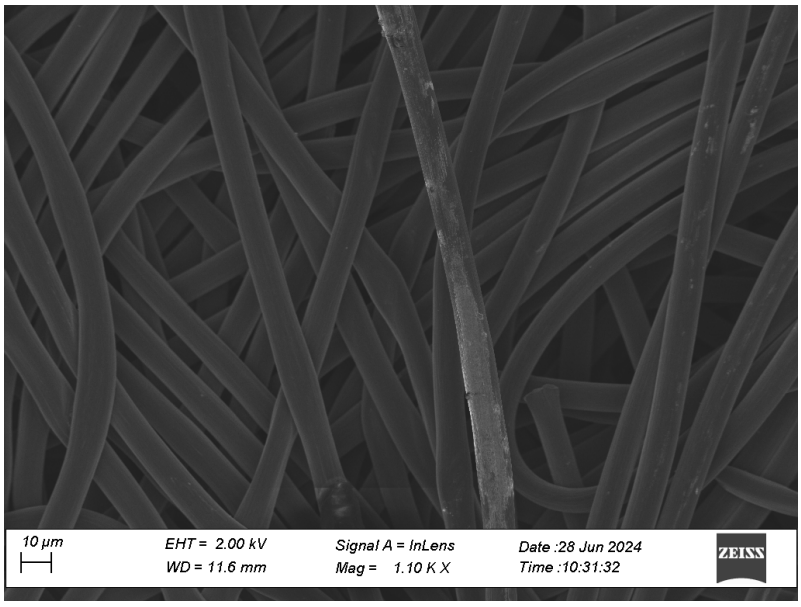

Figure 2.5: SEM image of wet laid F-H23

3
Methodology

3.0.1 Thermo-Gravimetric Analysis (TGA)

Thermogravimetric Analysis (TGA) is a thermal analysis technique that measures changes in the mass of a material as a function of temperature or time under a controlled atmosphere. This method is widely used to assess the thermal stability, composition, and decomposition characteristics of materials. During a TGA experiment, the sample is heated at a controlled rate, and the mass is continuously recorded, which allows for the identification of temperature ranges where the material undergoes significant changes such as moisture loss, decomposition, or oxidation.[15]
In this study, TGA was employed to evaluate the thermal stability and decomposition characteristics of the polytetrafluoroethylene (PTFE) dispersion used for hydrophobic treatment. The TGA measurements were conducted under atmospheric conditions with a heating rate of 10°C/min. The primary objective of this analysis was to determine the melting temperature and decomposition temperature of PTFE within the dispersion. These thermal properties are critical for understanding how the PTFE behaves during the hydrophobic treatment process, particularly in terms of its stability and effectiveness at elevated temperatures.
8ml of 60wt% PTFE dispersion was taken in an aluminum crucible for this exper-

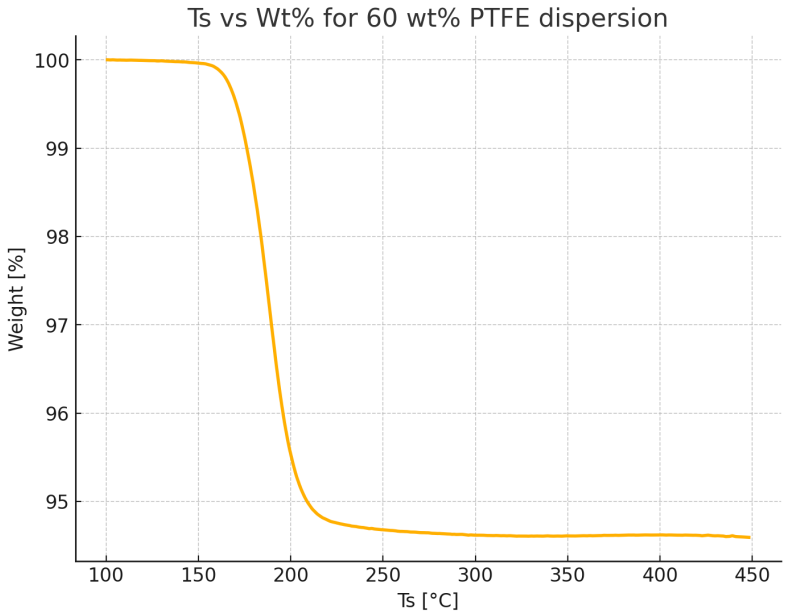

Figure 3.1: weight vs Temperature graph obtained using TGA

iment and from figure 3.1 its clearly seen that there has been a slight drop in the mass which indicates that the emulsion and water in the dispersion have been completely removed leaving the PTFE particles which have been stable upto 450 degree celsius.

3.0.2 Hydrophobic Treatment of GDLs

In this study, the hydrophobic treatment of Gas Diffusion Layers (GDLs) was performed using polytetrafluoroethylene (PTFE) dispersions at various concentrations, using a dip coating method. The below flow chart gives an insight into the step by step process involved follwed by the theoretical explanation of the process-

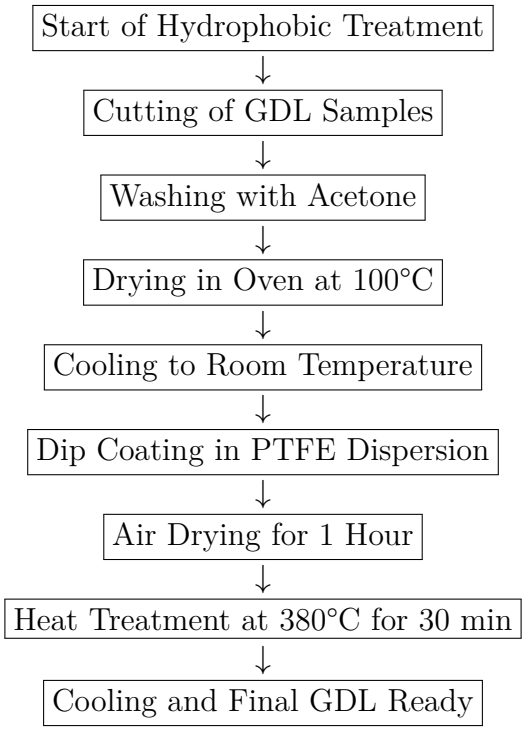

The GDL materials selected for this process were **SGL 39AA** (Dry-laid) and **Freudenberg H23** (Wet-laid) GDLs (purchased from Fuel Cell Store), chosen for their distinct manufacturing processes. These differences provide a comparative basis for evaluating the impact of hydrophobic treatment on different GDL structures. The objective of the hydrophobic treatment was to enhance the water-repellent properties of the GDLs, improving performance by preventing water accumulation and ensuring efficient gas diffusion.

3.0.3 Preparation of PTFE Dispersions

To achieve the required PTFE concentrations for the treatment, a commercial 60 wt% PTFE dispersion (purchased from Sigma Aldrich, consisting of PTFE particles 200-500nm in size, dispersed in alcohol solution) was diluted with deionized water

to achieve target concentrations of 5 wt%, 20 wt%, and 50 wt%. The dilution process was carefully controlled to ensure uniformity. Using the dilution formula[16], $C_1V_1 = C_2V_2$, where C_1 and V_1 represent the concentration and volume of the stock solution, and C_2 and V_2 represent the desired concentration and volume of the final solution, 3-5 mL of the 60 wt% PTFE dispersion was diluted with deionized water in clean containers to achieve the desired concentrations.

3.0.4 Preparation of GDL Substrates

The GDL substrates were prepared from hydrophilic carbon papers, ensuring that they were in optimal condition for hydrophobic treatment:

1. **Cutting**: The GDLs were cut into uniform pieces to ensure consistency in size and shape. This was critical for maintaining consistency in treatment and analysis.
2. **Washing**: The cut GDL pieces were washed in 90 mL of acetone to remove surface contaminants such as dust, or residues that could interfere with the PTFE coating. The washing was done by immersing the GDLs in acetone and gently agitating them for cleaning efficiency [17].

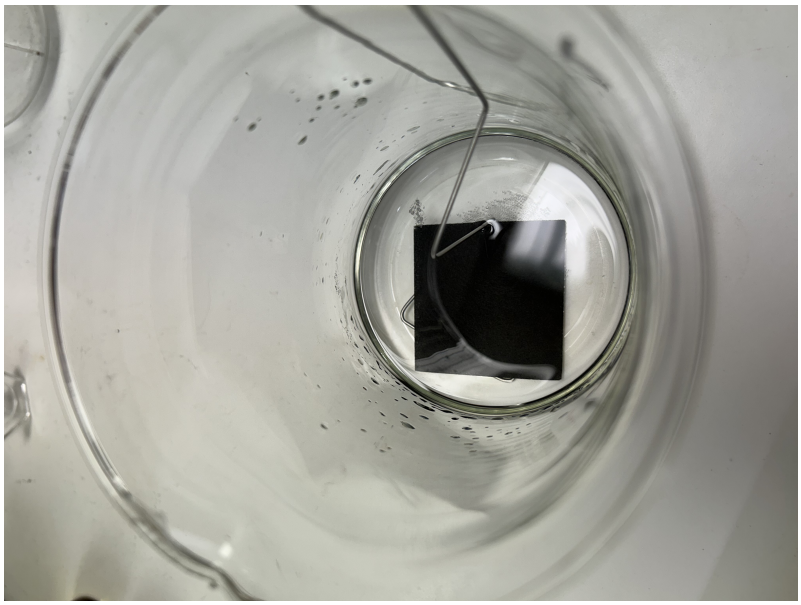

Figure 3.2: Washing of GDL in acetone solution, external force was applied with a steel wire due to high porosity of the GDL.

3. **Resting and Drying**: After washing, the GDLs were rested for 10 minutes to allow acetone to evaporate. The GDLs were dried in a calcination oven at 100°C for 1 hour to remove any remaining acetone or moisture.
4. **Cooling**: The dried GDLs were cooled to room temperature for 30 minutes.

3.0.5 Hydrophobic Treatment Process

The hydrophobic treatment was conducted by immersing the GDL substrates in diluted PTFE dispersions. Immersion times were carefully controlled to ensure a

consistent coating:

1. **Immersion**: The cooled GDL substrates were immersed in the PTFE dispersions. For 5 wt% PTFE, the immersion time was set at 30 seconds. For 20 wt% and 50 wt%, the immersion time was reduced to 15 seconds to prevent excessive PTFE deposition, which could clog the pores in the GDL structure.

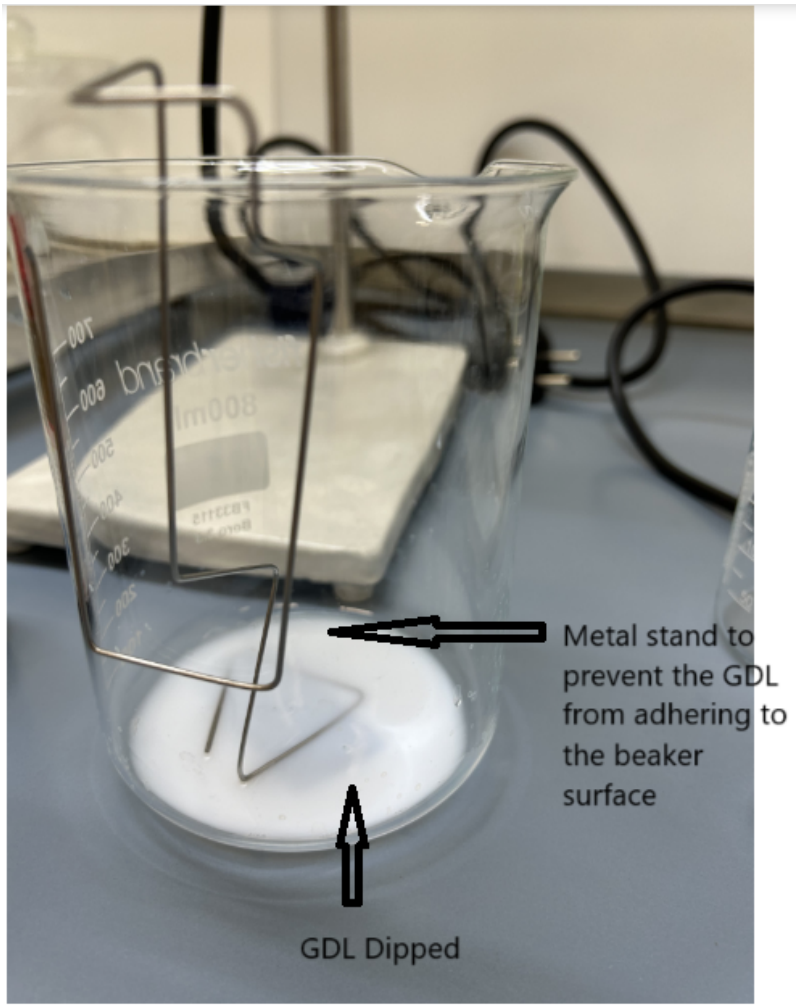

Figure 3.3: Dip coating of GDL in diluted PTFE Dispersion.

2. **Drying**: After immersion, the PTFE-coated GDLs were dried at room temperature for 1 hour. This allowed PTFE particles to loosely adhere to the GDL surface before heat treatment.
3. **Heat Treatment**: The GDLs were heat-treated from room temperature to 380°C, which approximately took 10 minutes and then stayed there for 20 minutes. This temperature was selected based on TGA analysis, ensuring the removal of the emulsion in the PTFE dispersion and optimal sintering of PTFE particles onto the GDL surface, forming a durable hydrophobic layer.
4. **Cooling**: The GDLs were cooled to room temperature gradually over 30 minutes to avoid thermal stress.

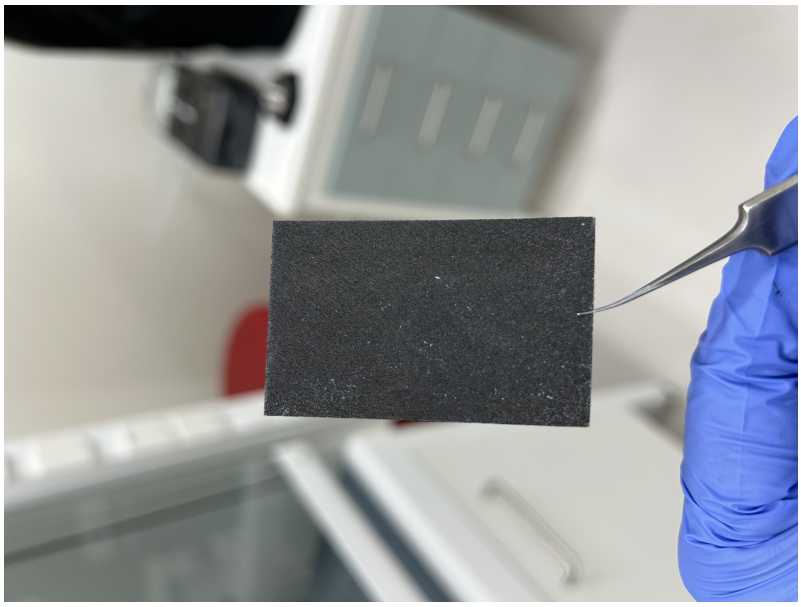

Figure 3.4: Dip-coated and dried GDL showing PTFE accumulations (white spots), which disappear after sintering.

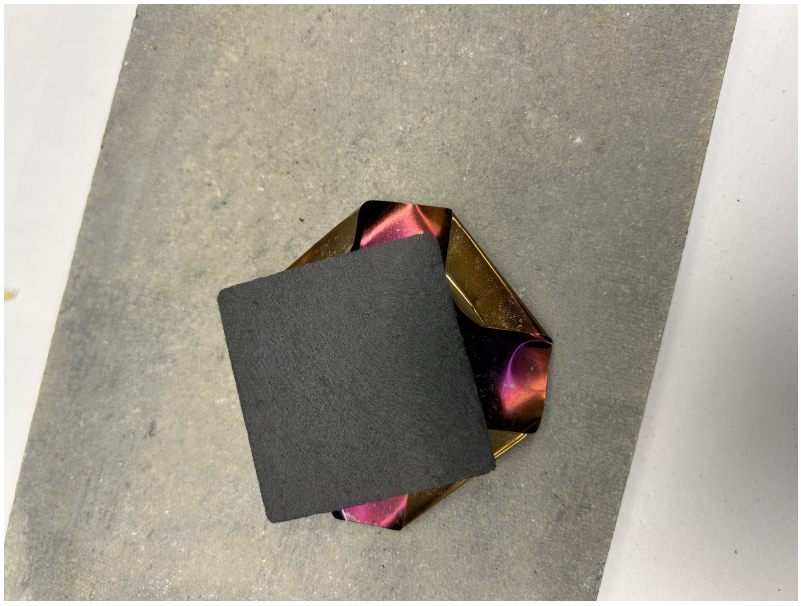

Figure 3.5: Heat-treated GDL showing uniform PTFE distribution, using a steel stand to prevent contamination.

3.0.6 PTFE wt% Calculation

After the hydrophobic treatment, the PTFE content was calculated by measuring the difference in mass before and after treatment. The weight gain was used to calculate the PTFE content as a percentage:

1. **Initial Weighing**: The untreated GDLs were weighed using a high-precision balance to record their initial mass.
2. **Post-Treatment Weighing**: The GDLs were re-weighed after the hydropho-

bic treatment to determine the mass of incorporated PTFE.

3. **Calculations**:
   - **Weight Gain**: The weight gain due to PTFE treatment was calculated as follows:

$$\text{Weight Gain} = \text{Mass after Treatment} - \text{Initial Mass}$$

   - **Weight Percentage of PTFE**: The PTFE content was calculated using the formula:

$$\text{Weight \% of PTFE} = \left(\frac{\text{Weight Gain}}{\text{Initial Mass}}\right) \times 100$$

3.0.7 PTFE wt% Calculation for SGL 39AA and Freudenberg H23

The tables 3.1 and 3.2 show the calculated PTFE wt% for both SGL 39AA and Freudenberg H23 GDLs after treatment, along with standard deviation between each sample for each PTFE concentration.

Conc.	S.No	Init. Mass (g)	Mass After (g)	PTFE wt%	Std. Dev.	Avg. PTFE wt%
5 wt%	1	0.2596	0.2796	7.15	0.1461	7.25
5 wt%	2	0.2578	0.2786	7.46		
5 wt%	3	0.2633	0.2836	7.14		
20 wt%	1	0.2633	0.2836	19.9	0.5559	20.67
20 wt%	2	0.2543	0.3229	21.9		
20 wt%	3	0.3362	0.3190	20.2		
50 wt%	1	0.2500	0.5125	50.8	1.5338	48.79
50 wt%	2	0.2520	0.5167	47.5		
50 wt%	3	0.2563	0.4844	47.08		

Table 3.1: SGL 10AA PTFE Content

Conc.	S.No	Init. Mass (g)	Mass After (g)	PTFE wt%	Std. Dev.	Avg. PTFE wt%
5 wt%	1	0.1041	0.1096	5.01	0.2156	5.17
5 wt%	2	0.0999	0.1057	5.08		
5 wt%	3	0.0999	0.1052	5.03		
20 wt%	1	0.1089	0.1382	21.1	1.1167	19.53
20 wt%	2	0.1052	0.1301	19.2		
20 wt%	3	0.1027	0.1302	18.3		
50 wt%	1	0.1000	0.2478	57.5	2.2799	56.40
50 wt%	2	0.1044	0.2146	55.3		
50 wt%	3	0.1100	0.2550	56.8		

Table 3.2: SGL 39AA PTFE Content

Observation and Conclusion
From the data above, we observe that the actual PTFE content in both GDL types was higher and lesser than the target concentrations (5 wt%, 20 wt%, and 50 wt%). This discrepancy is likely due to factors such as immersion time and material porosity. The variance in PTFE content was slightly higher for Freudenberg H23, possibly

due to its more complex pore structure compared to the dry-laid SGL 39AA, which showed more uniform distribution.
The hydrophobic treatment process was effective in achieving the desired hydrophobicity in both GDLs, though further optimization could reduce variance, particularly for higher PTFE concentrations. Throughout the thesis the target loadings will be used instead of the achieved concentrations for better and ease of understanding.

3.0.8 Raman Spectroscopy

Raman Spectroscopy was utilized to characterize the distribution of polytetrafluoroethylene (PTFE) across both the surface and cross-section of the Gas Diffusion Layers (GDLs), specifically SGL 39AA and Freudenberg H23. The measurements were conducted using a Renishaw inVia Raman Microscope. The spectrometer, fitted with a 20× objective lens and 50×, a laser with a wavelength of 785nm was used, the laser power was set between 1 to 5% at the sample plane to avoid damaging the sample. Spectral acquisition was performed with an exposure time of 0.5 seconds per point, and each spectrum was averaged over three accumulations to improve the signal-to-noise ratio. The Raman spectra were collected over a range of 500–1800 cm^{-1}, focusing on the C–F symmetric stretching mode of PTFE at 734 cm^{-1} and the in-plane hexagonal vibrations of C–C in graphitic carbon at 1575 cm^{-1} [18]. Raman mapping was employed by acquiring a point-by-point spectra. The intensity of the PTFE and carbon peaks was integrated to generate spatial maps of their distribution. The RAMAN maps were preferentially performed with 50wt% samples due to the high PTFE content which is easier for mapping the preffered adhere ponits of PTFE in the GDL. Challenges such as the uneven surface of the GDL substrates were managed through careful focusing and dynamic adjustment of acquisition parameters. The Raman maps revealed non-uniform PTFE distribution, with larger agglomerates in unsintered GDLs, which spread out after sintering, consistent with previous studies(refer the paper used for reference). Overall, Raman Spectroscopy provided a detailed understanding of PTFE distribution within the GDLs, essential for evaluating the hydrophobic treatment's effectiveness.

3.0.9 Scanning Electron Microscopy (SEM)

Scanning Electron Microscopy (SEM) was employed at various stages of the hydrophobic treatment process to investigate the morphology of the Gas Diffusion Layers (GDLs). The SEM imaging was conducted using a Zeiss Ultra 55 scanning electron microscope, which provided high-resolution images of the GDL surfaces and cross-sections. Initially, SEM imaging was performed after dipping the GDLs into the PTFE dispersion to observe the initial surface morphology and how well the PTFE adhered to the carbon fibers. The SEM analysis also revealed the bonding of the PTFE and the initial binder in the GDLs, particularly in the case of SGL 39AA, where it was crucial to assess the interaction between the polymers and the fibers. Subsequently, SEM analysis was conducted on the sintered GDLs to examine both surface and cross-sectional morphologies after the hydrophobic treatment. The SEM images provided detailed information on the microstructure, porosity, and

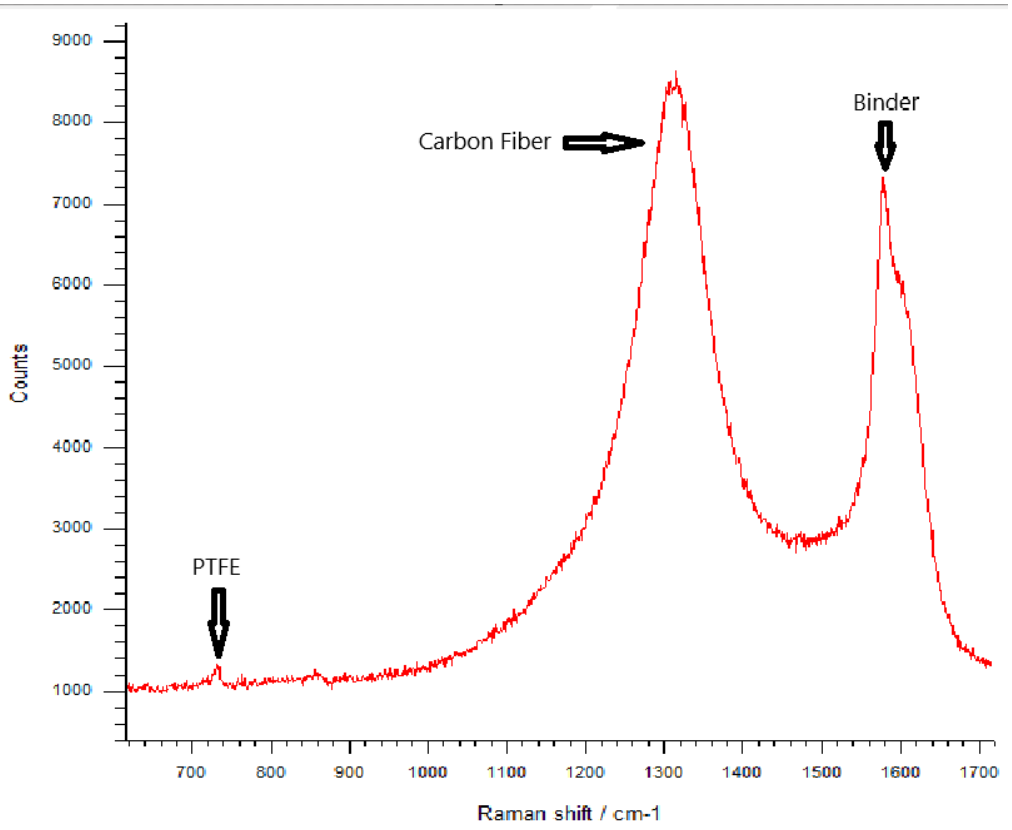

Figure 3.6: Spectral Acquisition of Hydrophobically treated GDL

distribution of PTFE particles within the GDLs. These observations were essential in understanding how the hydrophobic treatment affected the structural integrity and overall performance of the GDLs.

3.0.10 Energy Dispersive X-ray Spectroscopy (EDX)

Energy Dispersive X-ray Spectroscopy (EDX) was employed in conjunction with SEM to perform elemental analysis and verify the distribution of PTFE within the GDLs. EDX is a powerful technique that works by detecting characteristic X-rays emitted from the sample when it is bombarded with a focused electron beam within the SEM. These emitted X-rays correspond to specific energy levels unique to each element, allowing for the identification and spatial mapping of individual elements within the sample.

The underlying principle of EDX can be understood through an energy-level diagram of an atom. When the high-energy electron beam from the SEM interacts with the atoms in the sample, it transfers energy to the inner-shell electrons of those atoms, causing them to be excited to a higher energy state or completely ejected from the atom (ionization). This leaves a vacancy in the inner shell (typically the K or L shell). Electrons from higher energy levels (e.g., L or M shells) then drop down to fill this vacancy, releasing energy in the form of characteristic X-rays. The energy of these X-rays corresponds to the difference in energy levels between the two shells and is unique to each element.[3]

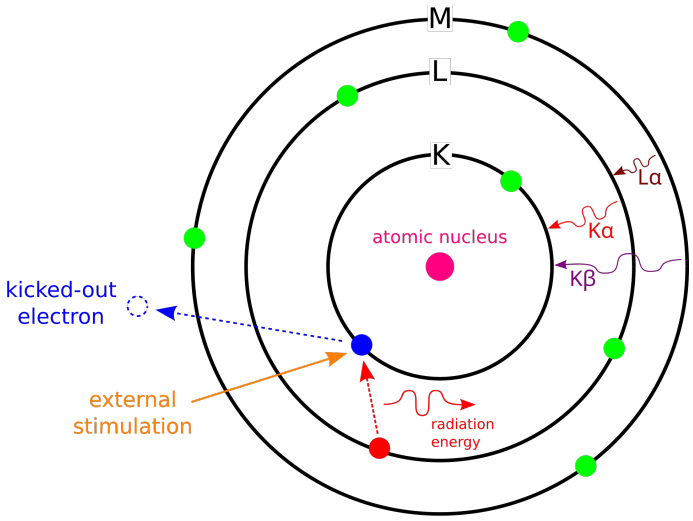

Figure 3.7: Schematic energy level diagram illustrating the excitation of an electron from the K shell and the emission of characteristic X-rays when an electron from the L shell fills the vacancy [3].image has been reproduced form the citation

In this study, EDX spectral acquisition was carried out on both the surface and cross-sectional areas of the GDLs to identify the presence and spatial distribution of elements, particularly fluorine, which is specific to PTFE. The detection of fluorine served as a direct indicator of PTFE distribution within the GDLs. This analysis was critical to verify the effectiveness of the hydrophobic treatment and to assess how uniformly the PTFE had been distributed across the GDLs.
To ensure the reliability of the elemental analysis, the EDX results were cross-verified with the spectral data obtained from Raman spectroscopy. This combination of SEM, EDX, and Raman spectroscopy provided a comprehensive understanding of the microstructure and elemental composition of the GDLs post-hydrophobic treatment, offering insights into the distribution of PTFE, carbon fibers, and other components across both the surface and internal sections of the GDLs.

3.0.11 Surface Contact Angle Measurement

Surface contact angle measurements were conducted using the sessile drop method to quantify the hydrophobicity of the GDLs treated with different concentrations (5 wt%, 20 wt%, and 50 wt%) of PTFE. The measurements were performed using a [specify the device] equipped with a high-resolution camera to capture the contact angle formed by a water droplet on the surface of each GDL sample. The sessile drop method involves placing a small droplet of water on the surface of the GDL and measuring the angle formed between the liquid-solid interface and the liquid-vapor interface. This angle is known as the contact angle, and it provides a direct measure of the surface's wettability.
The goniometer captures the droplet image as shown in figure 3.8, and specialized software analyzes the shape of the droplet to determine the contact angle. A reference line, often the baseline where the droplet meets the solid surface, is used to measure the angle between the tangent to the droplet surface and the solid surface

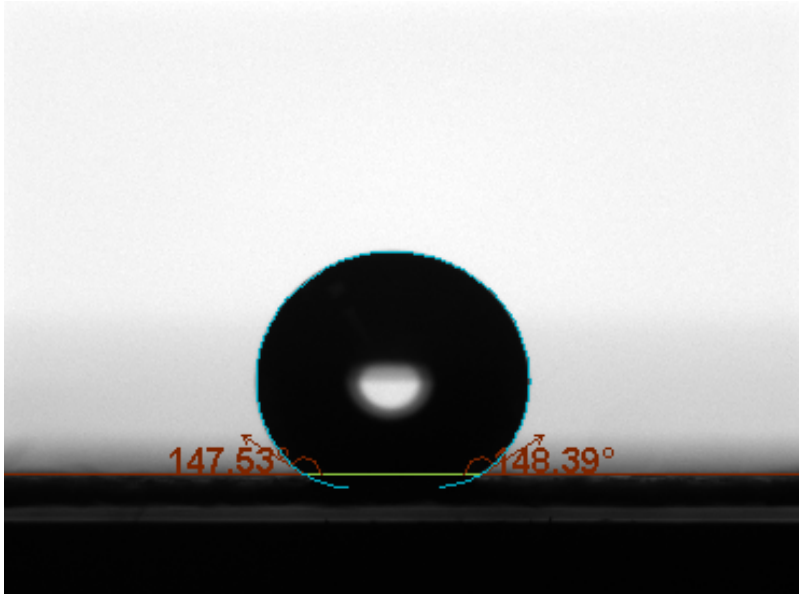

Figure 3.8: Surface contact angle measurement of F-H23 20wt% PTFE

at the contact point. The contact angle data were crucial for assessing how effectively the PTFE treatment altered the surface wettability of the GDLs, with higher contact angles indicating greater hydrophobicity.
The analysis also considers the Young-Laplace equation, which describes the balance of forces at the contact point and is crucial for understanding the equilibrium shape of the droplet. The Young-Laplace equation relates the contact angle (θ) to the surface tensions at the solid-liquid (γ_{SL}), liquid-vapor (γ_{LV}), and solid-vapor (γ_{SV}) interfaces through the equation [19]:

$$\cos\theta = \frac{\gamma_{SV} - \gamma_{SL}}{\gamma_{LV}}$$

This relationship helps explain how surface treatments like PTFE can alter the contact angle by modifying the surface tension at the solid-liquid interface, If $0 \leq \theta < 90°$ then the material is hydrophilic and hydrophobic if $90° < \theta \leq 120°$. The material is said to be superhydrophobic if the contact angle $\theta > 120°$ and the material gets fully wetted if the contact angle is $\theta = 0°$. By comparing the contact angles across the GDL samples treated with different PTFE concentrations, the effectiveness of the hydrophobic treatment in enhancing the water-repellent properties of the GDLs was quantitatively evaluated.

3.0.12 In-situ measurements

The toal gas transport resistance (R_T) in Gas Diffusion Layers (GDLs) was quantified using the dry limiting current method[9], an essential approach for investigating how the microstructure and material properties of GDLs influence oxygen transport in polymer electrolyte membrane (PEM) fuel cells. This method isolates the specific contribution of the GDL and the flow field plates to the overall transport resistance within the fuel cell, enabling precise enhancements in GDL design for improved per-

formance. These measurments were carried out at Powercell using a test station based on the operating conditions in table 3.1

Table 3.3: Operating Conditions for In-Situ Measurements

Parameter	Value
Operating Temperature	70°C
Cell Voltage Steps	0.35V to 0.1V with 0.05V steps and 2 min dwell time
Gas Humidification	70% RH
Pressure	300 kPa, 200 kPa, 150 kPa
Dry Mole Fraction of Oxygen	4%, 2%, 1%, 0.05%

This study employed two types of GDLs: the dry-laid SGL 39AA and the wet-laid Freudenberg H23. Each GDL was treated with varying amounts of polytetrafluoroethylene (PTFE) at concentrations of 5 wt%, 20 wt%, and 50 wt% to assess how these modifications affect oxygen transport resistance.[10]
The experimental process began with generating polarization curves by plotting current density against cell voltage. From these polarization curves, the limiting current densities (i_{lim}) were identified as shown in Figure 3.8, reflecting the maximum current that the cell could sustain under oxygen-limited conditions.

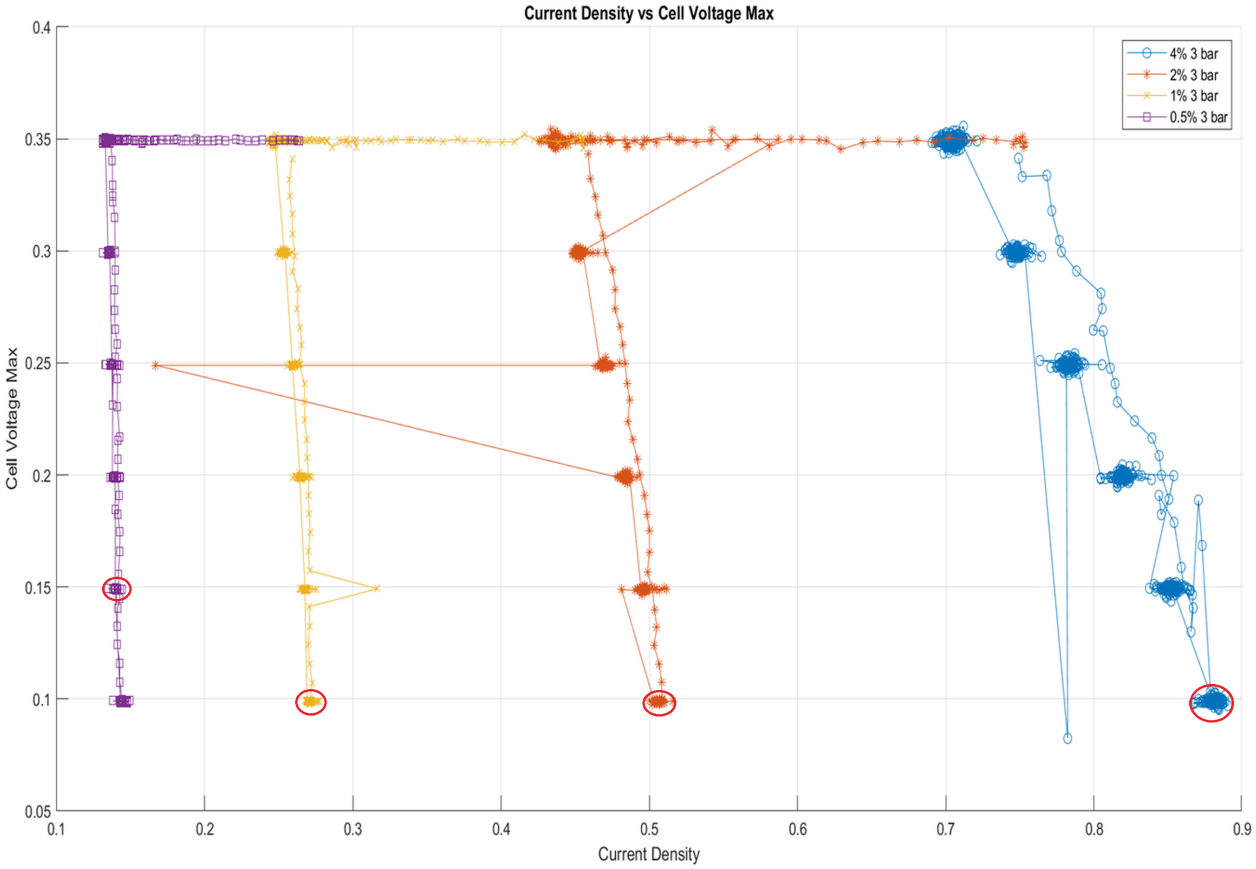

Figure 3.9: Polarisation curve with limiting currents marked for different oxygen concentrations at 300Kpa

The limiting current was then plotted against the oxygen concentration at different pressures to create i_{lim} versus O_2 concentration curves. The slope of these curves was crucial for subsequent calculations, as it was inserted into the formula for determining oxygen transport resistance:

$$R_T = \frac{4F x_O^{\text{dry-in}}}{i_{\text{lim}}} \cdot \frac{p - p_w}{RT}$$

where:

- F is Faraday's constant,
- $x_O^{\text{dry-in}}$ is the mole fraction of oxygen in the dry inlet gas,
- p is the total pressure,
- p_w is the water vapor pressure,
- R is the universal gas constant,
- T is the absolute temperature.

Subsequently, R_T was plotted against the pressure for each GDL. A linear fit was applied to the R_T versus pressure data, with the gradient of the resulting linear equation providing insights into the pressure-dependent component of the oxygen transport resistance[20]. The observation of pressure dependence highlights the complex interplay between gas diffusion mechanisms and the GDL's porous structure.

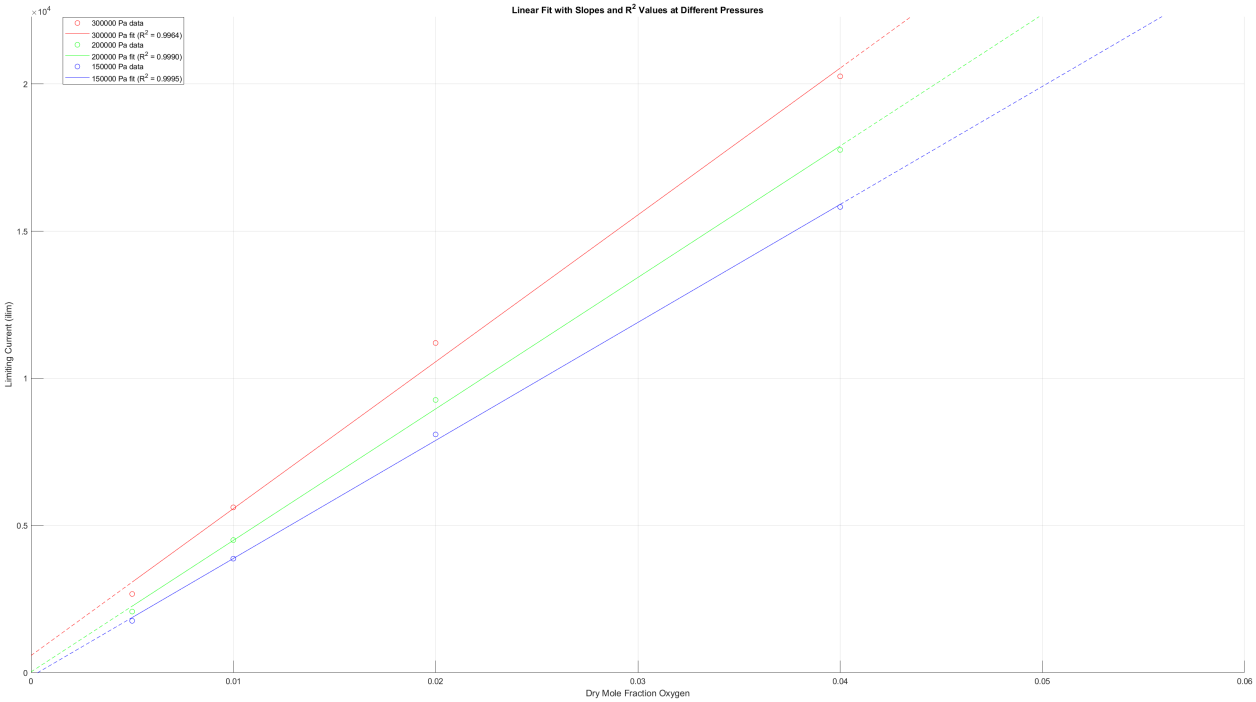

Figure 3.10: i_{lim} vs Oxygen concentration curve for SGL39AA 5wt%

At higher pressures, gas density increases, which enhances molecular collisions and could potentially influence the overall resistance to oxygen transport. This effect is especially significant in smaller pores where Knudsen diffusion dominates, leading to an increase in resistance as pressure rises. Knudsen diffusion, characterized by the interaction between gas molecules and the pore walls, becomes more prevalent when

the mean free path of the oxygen molecules is on the same order of magnitude as the pore size. Under these conditions, the resistance to oxygen transport is heavily influenced by the frequency of collisions with the pore walls, a phenomenon that becomes more pronounced as the pressure—and therefore the number of collisions—increases.
The diffusion of oxygen through the Gas Diffusion Layer (GDL) in a fuel cell is influenced by two primary mechanisms: molecular diffusion and Knudsen diffusion. The dominance of either mechanism depends on the relationship between the pore size within the GDL and the mean free path of the oxygen molecules.
Molecular diffusion occurs when the pores are relatively large compared to the mean free path of the oxygen molecules. In this regime, oxygen molecules primarily collide with each other as they move through the Gas Diffusion Layer (GDL). This type of diffusion is dominant when the pore sizes are on the order of micrometers or larger, making it the primary mode of oxygen transport in GDLs with larger pores.
The relationship between pore size and the mean free path is quantitatively described by the **Knudsen number (Kn)**, which governs the transition between different flow regimes [21]. The Knudsen number is defined as:

$$\mathrm{Kn} = \frac{\lambda}{d}$$

Where:

- λ is the mean free path of the gas molecules (i.e., the average distance a molecule travels before colliding with another molecule),
- d is the characteristic dimension of the pores in the GDL (e.g., the pore diameter).

The Knudsen number allows us to distinguish between different diffusion mechanisms, as follows:

- **Kn $<$ 0.01: Continuum Flow (Molecular Diffusion)** – When the pore sizes are much larger than the mean free path, molecular diffusion dominates. In this regime, oxygen molecules predominantly collide with each other. This is typical in GDLs with larger pores, where molecular diffusion is the primary mode of gas transport.
- **0.01 $<$ Kn $<$ 1: Transition Flow** – In this regime, both molecular diffusion and Knudsen diffusion occur simultaneously. The transport of oxygen is influenced by both intermolecular collisions and collisions with the pore walls.
- **Kn $>$ 1: Knudsen Diffusion** – When the pore sizes are smaller than the mean free path, Knudsen diffusion becomes dominant. In this regime, oxygen molecules are more likely to collide with the pore walls than with each other. This occurs in GDLs with very small pores, typically on the nanometer scale, where Knudsen diffusion governs the gas transport.

In summary, the Knudsen number provides a useful framework for understanding the interplay between molecular and Knudsen diffusion in GDLs. The overall transport properties of the GDL are determined by the interplay between molecular and Knudsen diffusion mechanisms. At higher pressures and in GDLs with larger pores, molecular diffusion generally dominates. Conversely, at lower pressures or in GDLs with smaller pores, Knudsen diffusion becomes more significant[22]. The degree of PTFE loading can further influence this balance by altering the effective pore size.

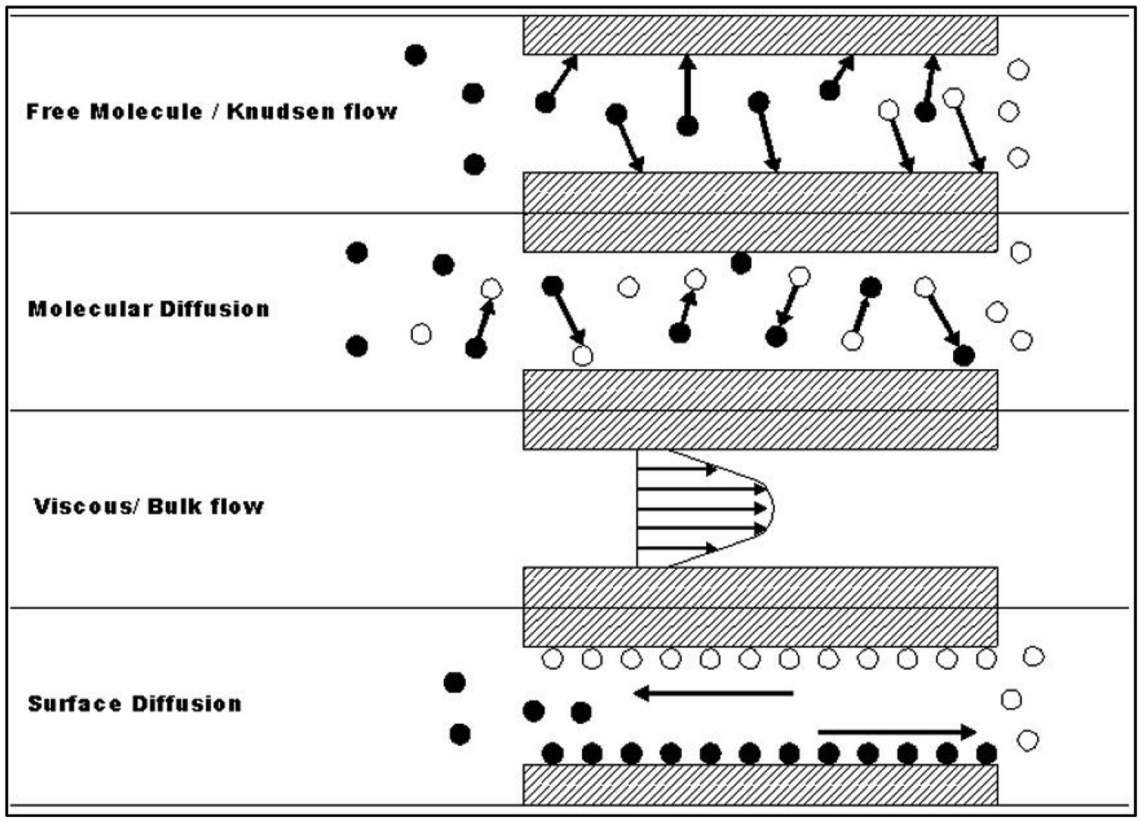

Figure 3.11: Types of mass transport through gas diffusion layer [4] image reproduced from the citation

In this study, the PTFE appears to modify the pore structure in a way that increases the prevalence of Knudsen diffusion. As PTFE accumulates and reduces the effective pore size, collisions between gas molecules and the pore walls become more frequent, thus making Knudsen effects non-negligible. This is reflected in the measured total transport resistances, where higher PTFE concentrations result in increased oxygen transport resistance, indicating a shift towards Knudsen-dominated transport.
To ensure accurate measurement of oxygen transport resistance, the experimental setup was meticulously controlled to prevent water condensation within the cell. Liquid water could obstruct the pores and significantly alter the GDL's effective transport properties, leading to erroneous resistance measurements[23]. Operating the cell under dry conditions ensures that the observed transport resistance was due solely to the GDL's inherent structure and PTFE treatment, without interference from liquid water.
These findings emphasize the importance of considering pressure as a key factor in the design and optimization of GDLs. Understanding how oxygen transport resistance changes with pressure is crucial for designing GDLs that perform efficiently across a range of operating conditions. By tailoring the microstructural properties of GDLs, it is possible to achieve an optimal balance between hydrophobicity, oxygen transport efficiency, and pressure-dependent behavior, thereby enhancing overall fuel cell performance[24].

4

Results

4.1 Contact Angle Measurements

The contact angle measurements were performed on the Gas Diffusion Layers (GDLs) treated with different concentrations of polytetrafluoroethylene (PTFE) to assess their hydrophobicity. The results, summarized in Table , show the contact angles for both Freudenberg H23 (wet-laid) and SGL 39AA (dry-laid) GDLs at PTFE concentrations of 5 wt%, 20 wt%, and 50 wt%.

PTFE wt%	Contact angle (F-H23) Average	Contact angle (SGL 39AA) Average	Standard deviation
5	138.66	137.60	0.5
20	144.92	146.14	0.6
50	145.96	146.98	0.5

Table 4.1: Contact angles and standard deviations for different PTFE wt% values

Discussion:

As the PTFE content increased from 5 wt% to 50 wt%, the contact angle of water on the GDL surface also increased, indicating enhanced hydrophobicity. This trend was consistent across both types of GDLs, with only slight variations in the contact angles between Freudenberg H23 and SGL 39AA. The increase in contact angle reflects the increased ability of the GDL surface to repel water, which is crucial in preventing flooding within the PEMFC.

However, the differences in contact angles between the 20 wt% and 50 wt% PTFE concentrations were relatively small, suggesting that the hydrophobicity of the GDL surface reaches a plateau at higher PTFE contents, this has been represented in figure 4.1. This plateau indicates a limit to the effectiveness of additional PTFE in further enhancing hydrophobicity, where further increases in PTFE concentration have diminishing returns on the contact angle.

The consistency between the two types of GDLs in their response to PTFE treatment suggests that the relationship between PTFE content and surface hydrophobicity is largely independent of the GDL manufacturing process. Both dry-laid and wet-laid GDLs exhibit similar enhancements in hydrophobicity with increasing PTFE content, highlighting the robustness of PTFE treatment as a method for improving water management in PEMFCs.

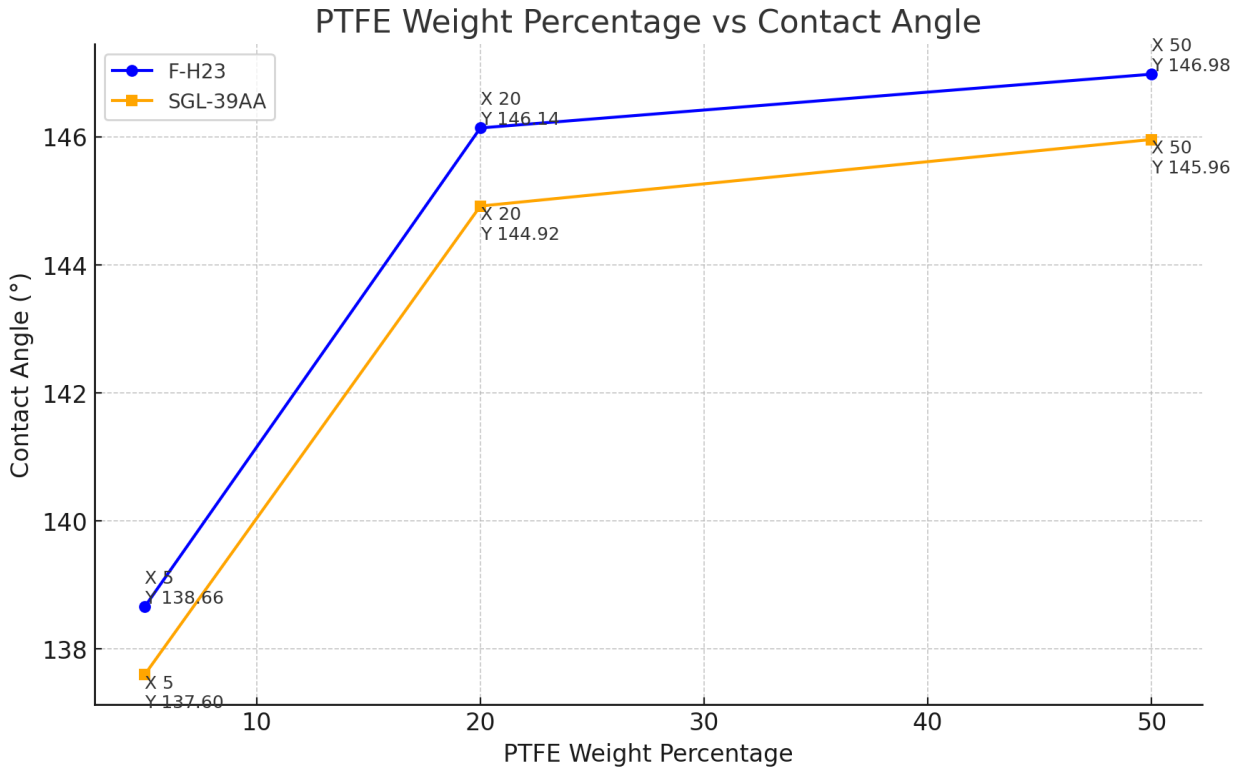

Figure 4.1: Contact angle vs PTFE wt% for both type of GDLs

4.2 Raman Spectroscopy

Raman spectroscopy was employed to map the distribution of PTFE within the GDLs, providing spatially resolved chemical information. This technique was particularly useful for identifying and mapping the PTFE, carbon fibers, and carbonaceous binder within the SGL 39AA GDL. The 50wt% samples were used for raman spectroscopy due to high density of PTFE except the crossection mapping for F-H23 GDL,were the 20wt% PTFE GDL was used. However, for SEM and EDX 20wt% PTFE GDLs were used.

4.2.1 SGL 39AA Findings

The Raman spectroscopy results for the SGL 39AA GDL revealed some unique challenges and insights. The Raman spectra successfully identified the presence of PTFE, carbon fibers, and the carbonaceous binder within the GDL. However, mapping the distribution of PTFE in the SGL 39AA was more difficult compared to the Freudenberg H23.

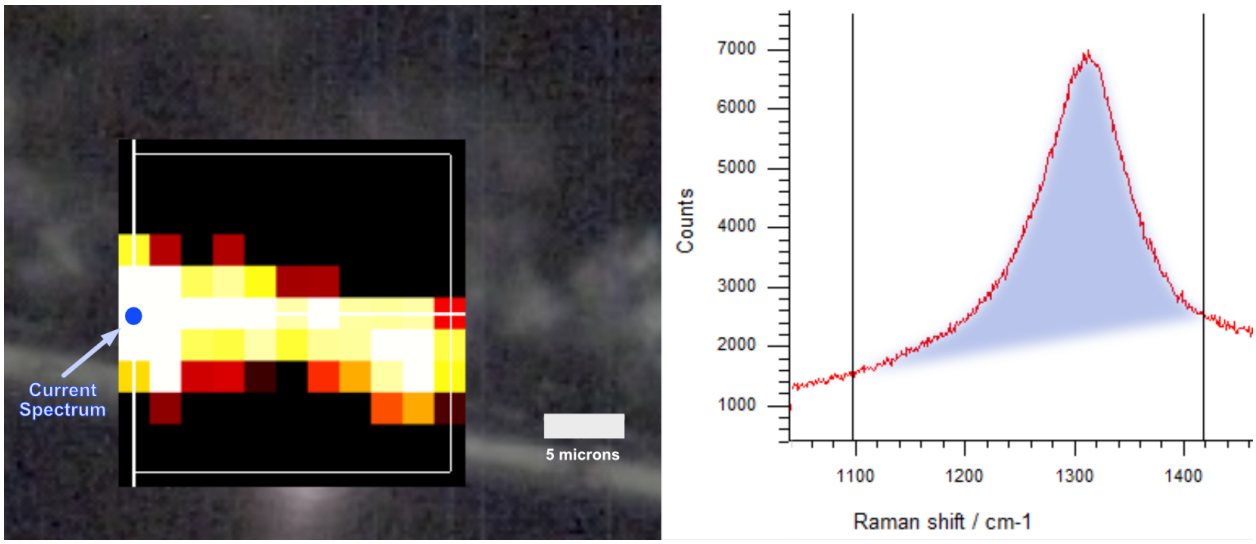

Figure 4.2: RAMAN Map of carbon fiber in SGL 39AA obtained by integrating the area below the intensity peak at 1300 cm^{-1}.

The difficulty arose from the PTFE's preferential adherence to the pores between the carbonaceous binder and the carbon fibers, rather than forming a uniform layer across the GDL surface. This behavior suggests that PTFE tends to localize in the less dense regions of the GDL, where it can fill the voids and adhere to the binder material. This localization could potentially create areas within the GDL that are either too hydrophobic, leading to poor gas diffusion, or insufficiently treated, leading to flooding.

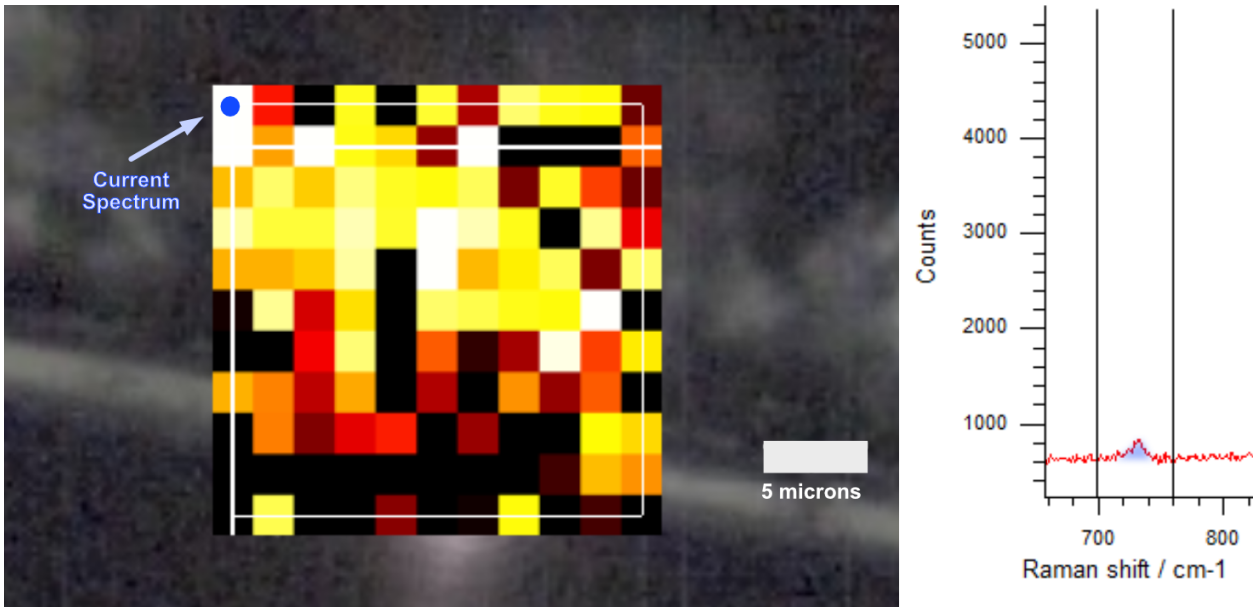

Figure 4.3: RAMAN Map of PTFE in SGL 39AA obtained by integrating the area below the intensity peak at 734 cm^{-1}.

Furthermore, unlike in Freudenberg H23, we were unable to map PTFE consistently across the cross-section of SGL 39AA. This lack of cross-sectional mapping

is puzzling and could be due to several factors, including the possible migration of PTFE away from the GDL during the sintering process or the limited penetration of PTFE into the deeper layers of the GDL. The inability to map PTFE across the cross-section raises concerns about the overall uniformity of PTFE distribution within the SGL 39AA GDL.

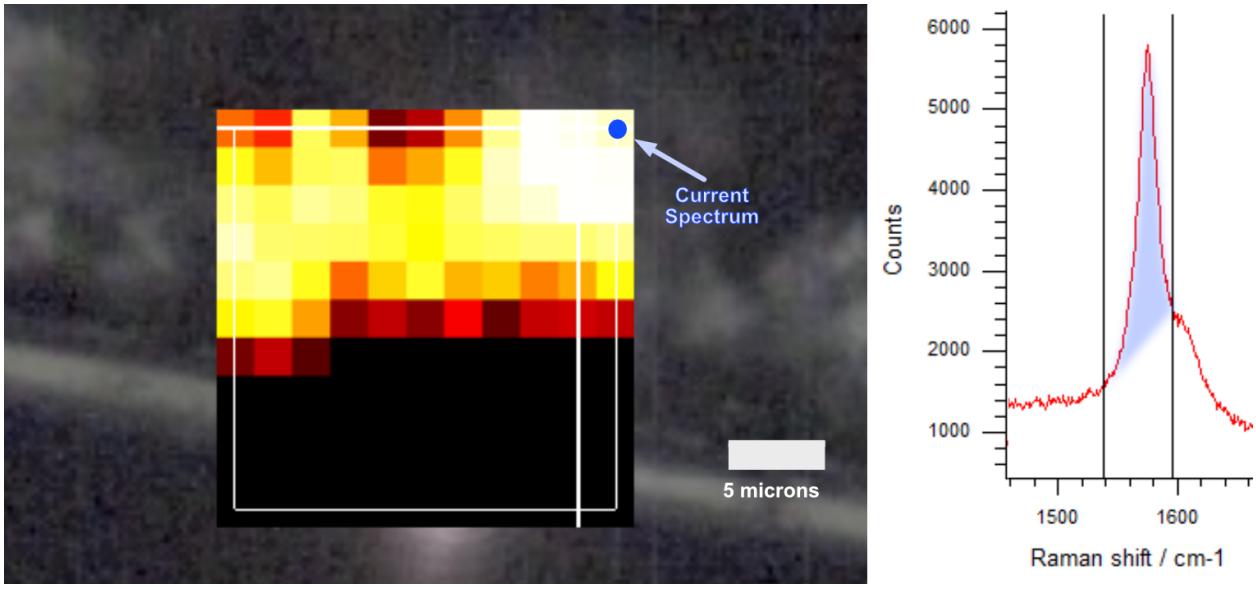

Figure 4.4: RAMAN Map of carbonaceous binder in SGL 39AA obtained by integrating the area below the intensity peak at 1575 cm^{-1}.

These Raman findings were corroborated by Energy Dispersive X-ray Spectroscopy (EDX) results, which showed poor intensity signals for fluorine, particularly in the deeper sections of the SGL 39AA GDL. The weak fluorine signals suggest that PTFE is not well distributed throughout the GDL, particularly in the areas that are crucial for gas transport and water management.

4.2.2 F-H23 Findings

For the Freudenberg H23 GDL with 50 wt% PTFE, the Raman maps showed concentrated areas of PTFE, which were identified by the intensity of the Raman peaks associated with PTFE. Similarly, the carbon fiber distribution was mapped, showing the locations of the fibers within the GDL. The overlap between the PTFE and carbon fiber maps indicated that PTFE was adhering to the carbon fibers, but with some variability in coverage.

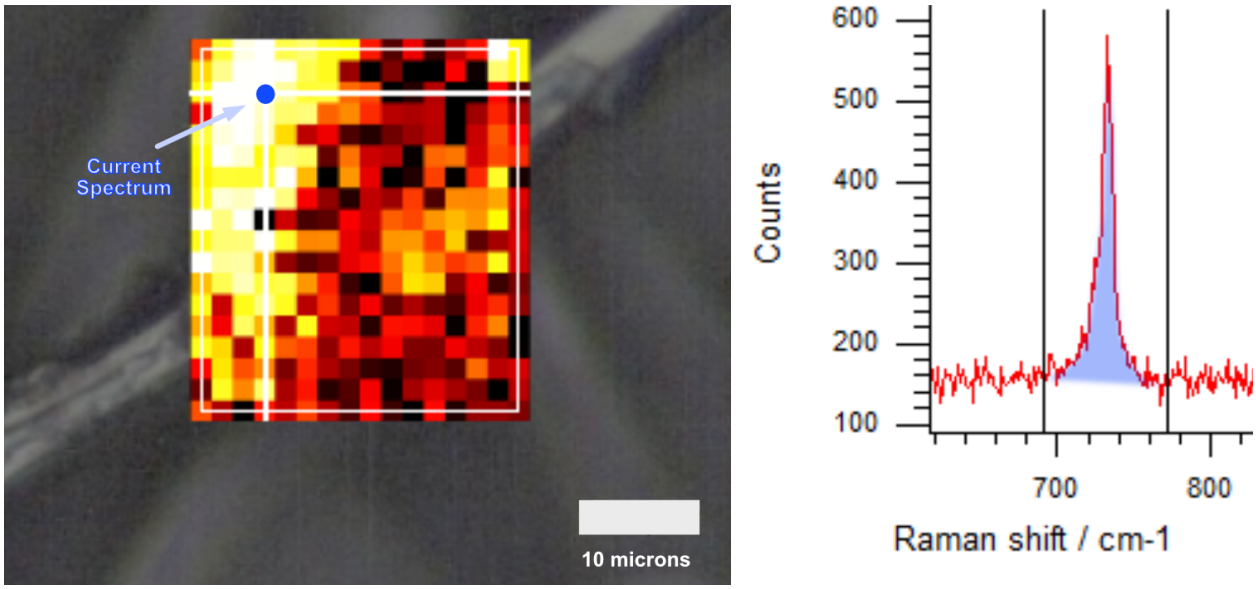

Figure 4.5: RAMAN Map of PTFE in F-H23 obtained by integrating the area below the intensity peak at 734 cm^{-1}.

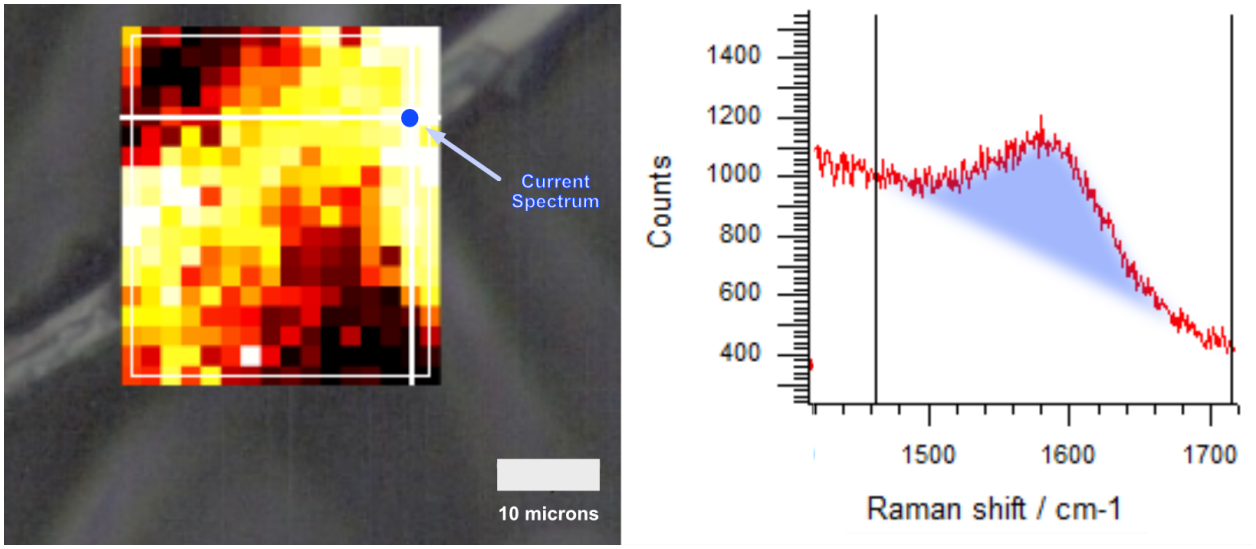

Figure 4.6: RAMAN Map of carbon fiber in F-H23 obtained by integrating the area below the intensity peak at 1300 cm^{-1}.

The cross-sectional mapping of the Freudenberg H23 GDL with 20 wt% PTFE demonstrated that PTFE was distributed throughout the GDL thickness, though with some non-uniformity. This variability in PTFE distribution could lead to uneven water management within the fuel cell, where regions with insufficient PTFE might be prone to flooding, while areas with excessive PTFE might impede gas transport.

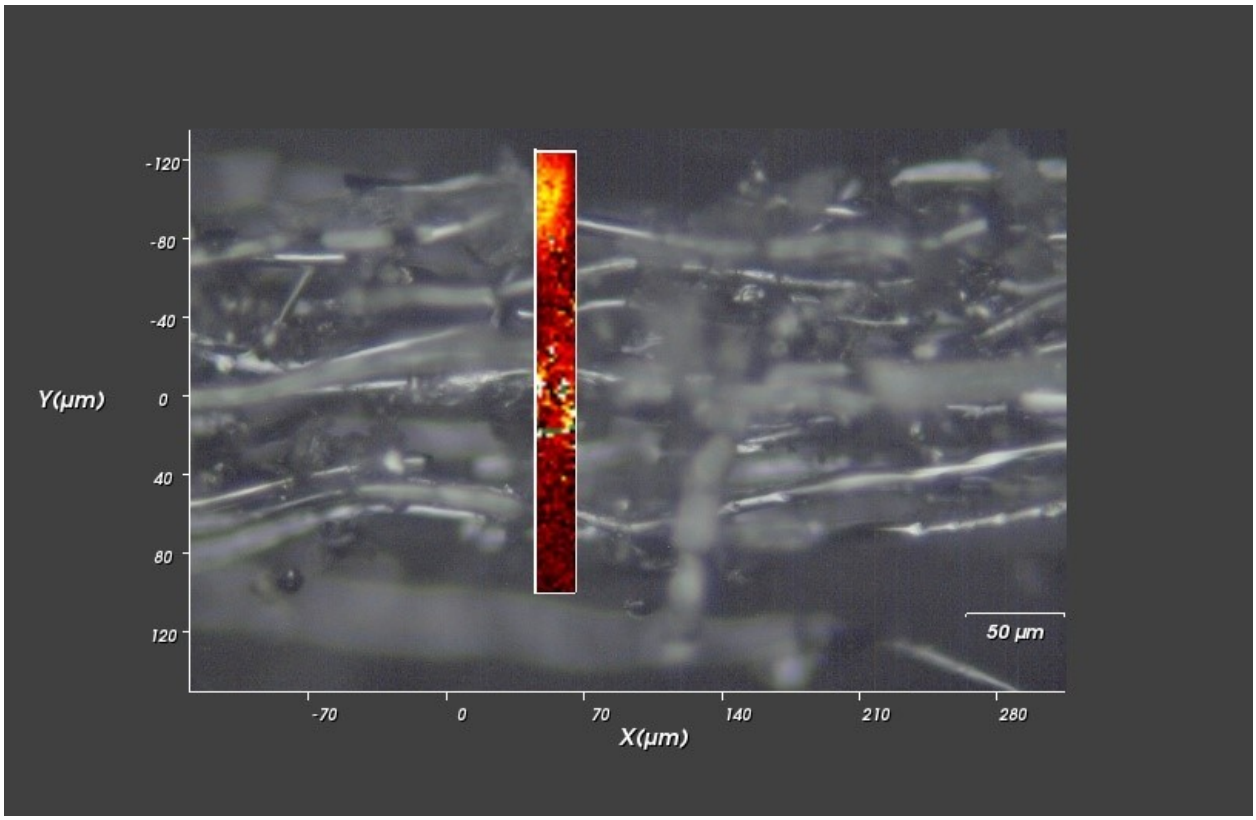

Figure 4.7: RAMAN Map of PTFE across the cross-section of cryo cut F-H23 GDL.

Implications for PEMFC Performance:
The non-uniform distribution of PTFE in SGL 39AA, as indicated by both Raman and EDX results, could have significant implications for PEMFC performance. Areas with insufficient PTFE may become prone to flooding, while areas with excessive PTFE may restrict gas transport, leading to uneven performance across the GDL. These issues underscore the importance of optimizing the PTFE application process, particularly for GDLs like SGL 39AA, to ensure a more uniform and effective distribution of the hydrophobic treatment.
In contrast, the Freudenberg H23 GDL showed more consistent PTFE distribution, particularly in the cross-sectional analysis. However, the challenge of achieving a perfectly uniform distribution remains. Future work should focus on refining the PTFE application methods to minimize these variations and improve the overall performance and durability of PEMFCs.

4.3 SGL 39AA SEM and EDX Analysis

Scanning Electron Microscopy (SEM) was employed to investigate the morphology of the SGL 39AA Gas Diffusion Layer (GDL) at various stages of the hydrophobic treatment process. Initially, SEM imaging was conducted on the untreated SGL 39AA GDL to establish a baseline for the surface and internal morphology. The images at lower magnifications (e.g., 144x) revealed a relatively uniform fiber network

with distinct pores primarily formed between the binders and at the fiber-binder interfaces. Higher magnification images (e.g., 1.10Kx) provided a closer look at the intricate pore structures and the distribution of the binder material. The untreated GDL showed no evidence of PTFE presence, as confirmed by the spectral acquisition, which showed no fluorine signals in the EDX analysis.

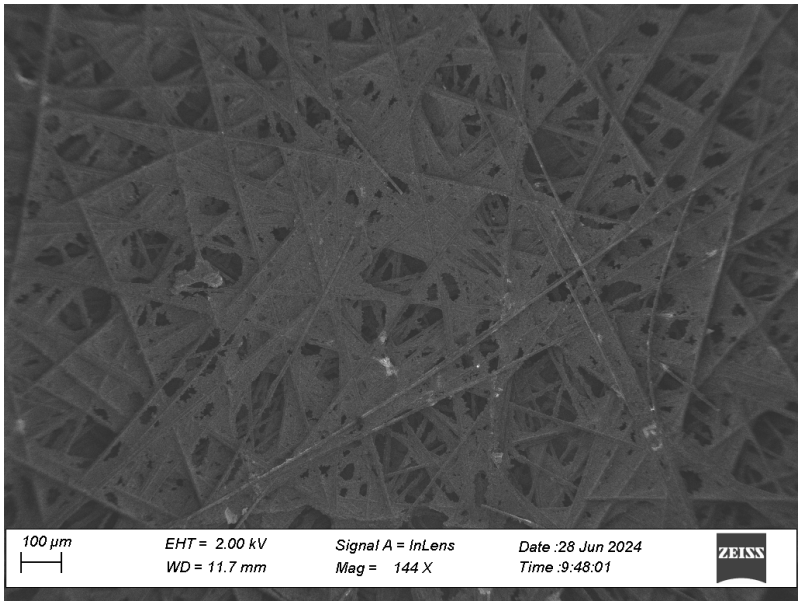

Figure 4.8: SEM image of untreated SGL 39AA GDL at 144Kx magnification, showing the fiber network and pore distribution.

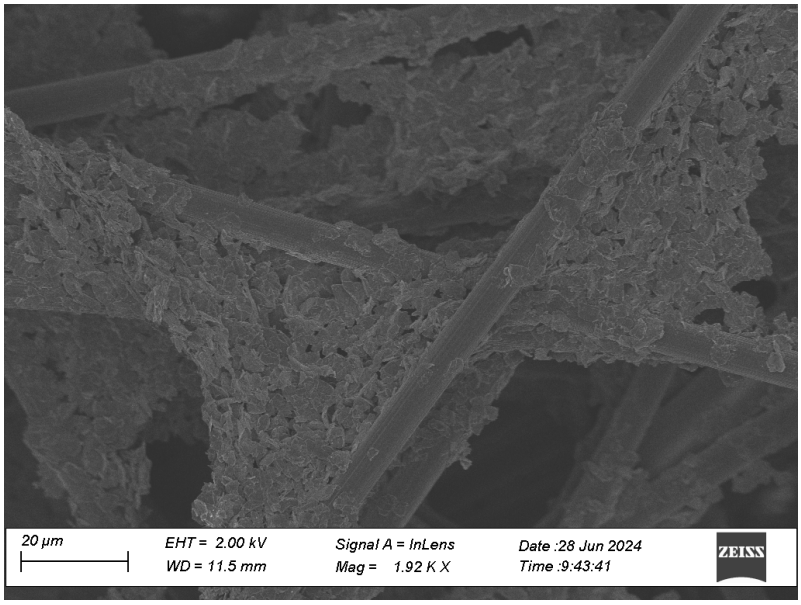

Figure 4.9: SEM image of untreated SGL 39AA GDL at 1.92Kx magnification, highlighting the binder and fiber interfaces.

After the dip-coating process with 20 wt% PTFE, SEM images revealed significant morphological changes in the SGL 39AA GDL. A significant difference can be noted

between Figures 4.8 and 4.10,the PTFE particles were observed to preferentially occupy the pores between the binder materials, as well as within the fiber-binder interfaces, rather than uniformly coating the fibers. This selective adherence of PTFE highlights the challenge of achieving a homogeneous hydrophobic coating across the GDL surface.

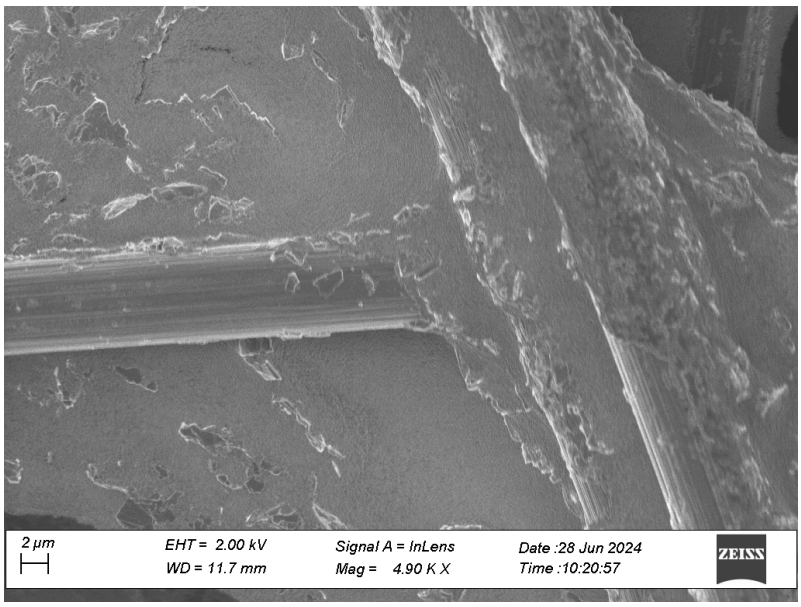

Figure 4.10: SEM image of dip-coated SGL 39AA GDL at 4.90Kx magnification, showing PTFE distribution within the binder pores.

Upon sintering, further SEM analysis showed that PTFE had successfully filled many of the pores, creating a more continuous coating over the GDL's surface. However, despite this improvement, the PTFE coverage was still not entirely uniform, with some areas showing higher concentrations of PTFE than others. This uneven distribution could potentially impact the GDL's effectiveness in managing water and facilitating gas transport within a PEMFC.

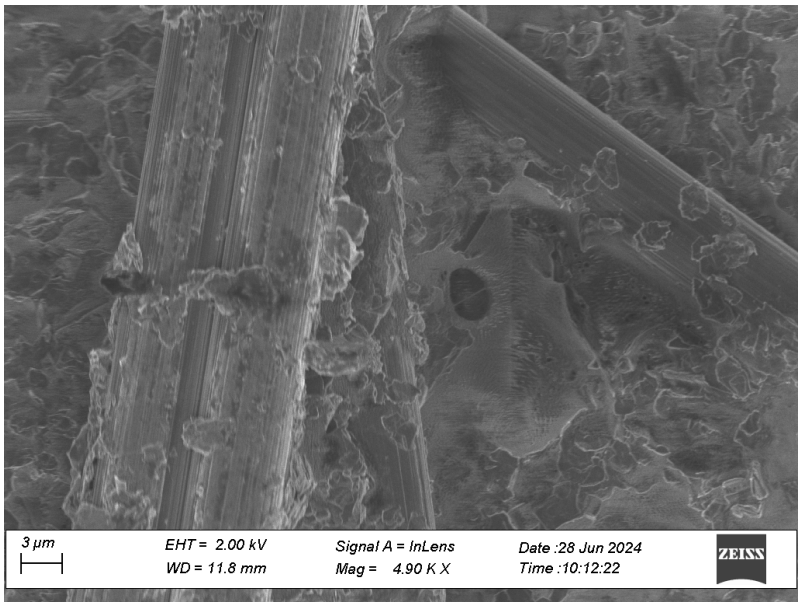

Figure 4.11: SEM image of sintered SGL 39AA GDL at 1.10Kx magnification, showing the distribution of sintered PTFE.

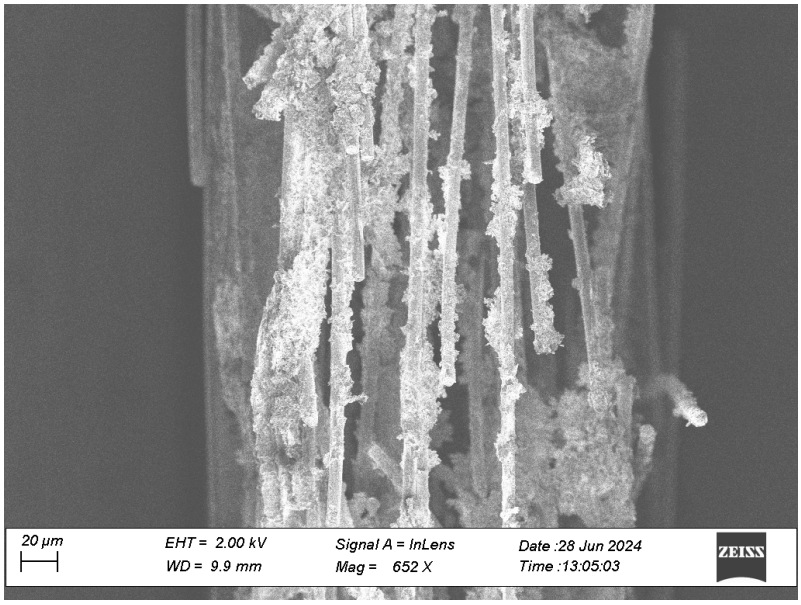

Figure 4.12: Cross-sectional SEM image of sintered SGL 39AA GDL, highlighting the challenges in characterising the PTFE distribution within the GDL thickness.

4.3.1 EDX Analysis SGL 39AA

Energy Dispersive X-ray Spectroscopy (EDX) was performed to verify the presence and distribution of PTFE within the SGL 39AA GDL. In the dip-coated samples, EDX confirmed the presence of fluorine, indicating PTFE adherence primarily within the binder pores. However, in the sintered samples, the EDX spectra revealed that

while PTFE was present, its distribution was still uneven, particularly in the cross-sectional analysis.
The weak fluorine signals detected in some regions suggest that PTFE did not penetrate deeply into the GDL or that it may have preferentially migrated during the sintering process, leaving some areas less protected against water intrusion.
The following images depict the SEM images that have been focused to obtain the spectrums for all the steps in the hydrophobic treatment process. The SEM image

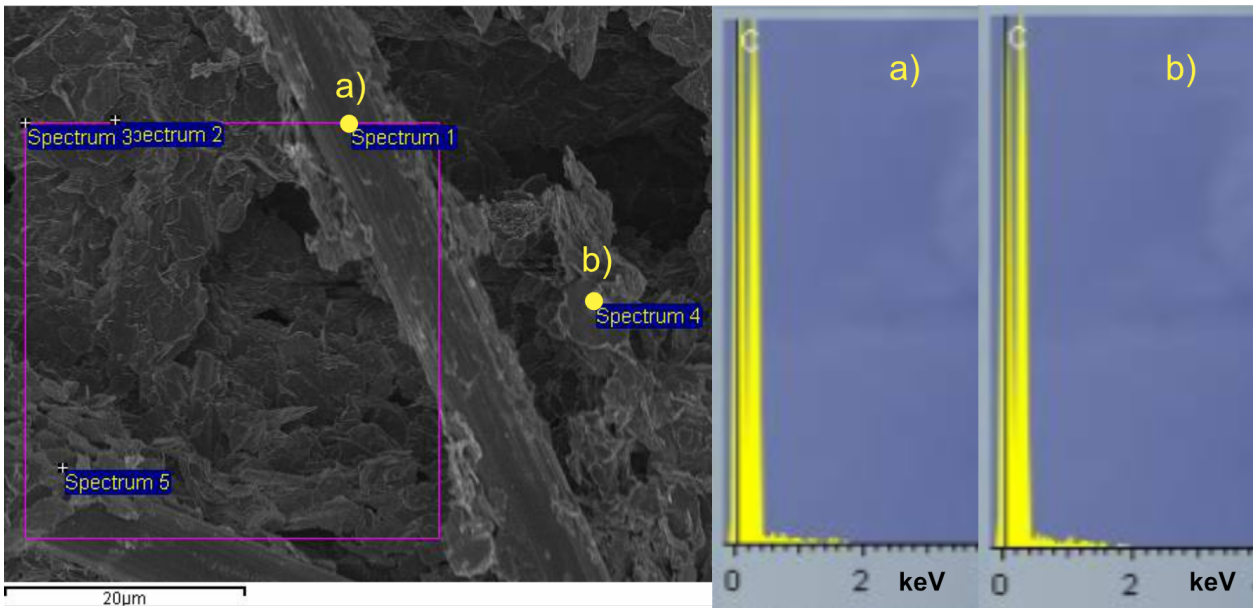

Figure 4.13: SEM image of initial SGL 39AA GDL with EDX spectrum spots at 4.85kx magnification

in Figure 4.13 was selected for EDX analysis because it includes both the fiber and binder regions, which allows for a comprehensive comparison of their chemical compositions.
Spectrum 1 (shown in Figure 4.13) was acquired from the fiber, and as expected, the EDX results show primarily carbon peaks, confirming that the fiber material is composed entirely of carbon, consistent with the fact that the GDL is made of carbon fibers.
Spectrum 4 was acquired from the binder region, and the results indicate that the binder is carbonaceous in nature, as expected. This was earlier confirmed by Raman spectroscopy analysis of the SGL 39AA samples with 56 wt% PTFE. The presence of only carbon peaks suggests that the binder is also composed of carbonaceous material, consistent with the expected composition of the GDL.
The comparison between Spectra 1 and 4 highlights the different regions of the GDL, showing that the carbon fiber and binder share similar elemental compositions, although their microstructures differ.

Following the initial analysis, the EDX analysis was continued on the dip-coated, unsintered SGL 39AA samples. This analysis confirmed that the PTFE particles and the emulsion tend to accumulate in the pores between the binder and in the fiber-binder interface, as observed in the SEM images. This accumulation can influence

the hydrophobicity and gas transport properties of the GDL, which will be analyzed further in subsequent sections.

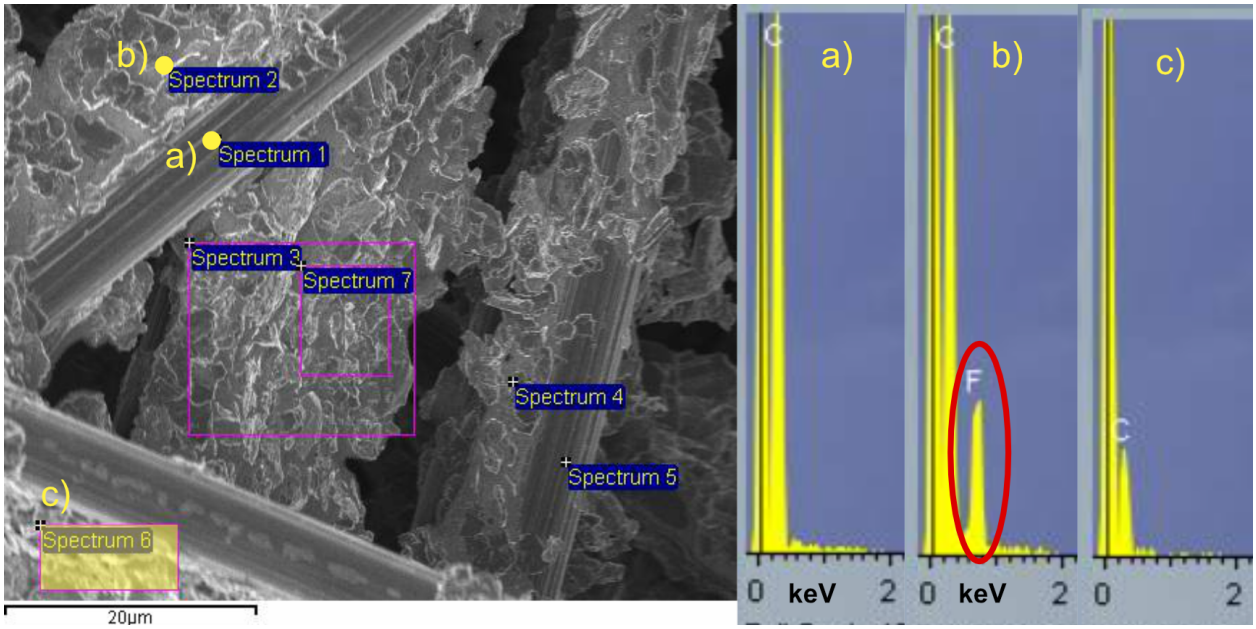

Figure 4.14: SEM image of dip coated SGL 39AA GDL with EDX spectrum spots at 4.85kx magnification

The spot was chosen as mentioned earlier due to the difference in figure 4.9 and 4.10, seven spectrums were done to see if the PTFE has been preferentially been accumulated between the pores of the binder out of these seven spectrums only spectrum 2 showed the presence of PTFE which is obvious as PTFE is not sintered. This shows that sinterring is an essential process for the PTFE to spread out accross and through the GDL.

The EDX analysis was continued with the sintered SGL 39AA samples to confirm if as seen from the dip coated unsintered SGL 39AA samples EDX analysis that the PTFE particles have spread out and have been accumulated between the pores in the binder and also between the fiber binder interface.

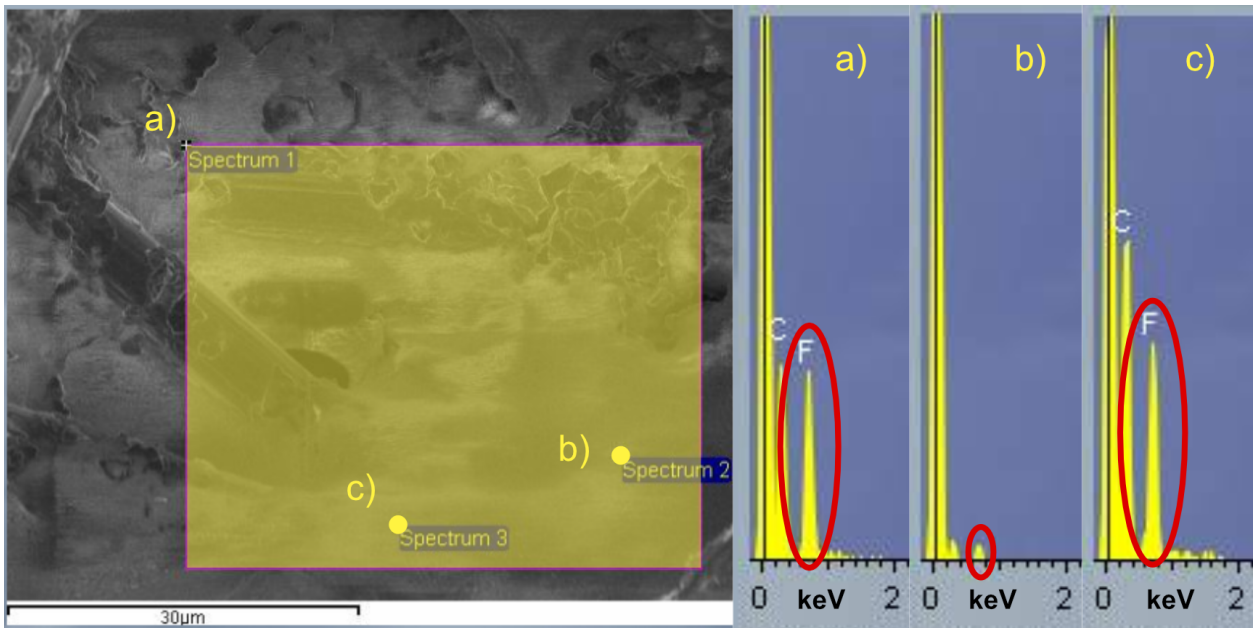

Figure 4.15: SEM image of sintered SGL 39AA GDL with EDX spectrum spots at 4.85kx magnification

The SEM spot was chosen for the same reason as previously mentioned: to investigate whether PTFE had accumulated within the binder pores and at the fiber-binder interface. **Spectrum 1**, shown in Figure 4.15, clearly indicates a high fluorine intensity, confirming the presence of PTFE in these regions.

Two additional point spectra were performed to assess whether the sintering process provided a uniform, homogeneous distribution of PTFE. **Spectrum 2**, depicted in Figure 4.15, reveals that even after sintering, the PTFE distribution is not homogeneous across the GDL.

From these spectra, it is evident that PTFE tends to accumulate in the binder pores and in the pores between the fiber-binder interface. This confirms that the hydrophobic treatment method is effective, as corroborated by the contact angle measurements. However, the lack of homogeneity after sintering suggests there is room for improvement in achieving a more even PTFE distribution.

This behavior of PTFE accumulation and partial non-homogeneous distribution could impact the overall gas transport and water management properties of the GDL in PEM fuel cells.

The EDX analysis was continued with the SGL 39AA 20wt% PTFE cross section samples, these samples were prepared carefully by cryo cutting method in which the GDLs were dipped in liquid nitrogen for a few seconds and were cut with a sharp scalpel immediately to avoid the destruction of the artifacts within the GDL.

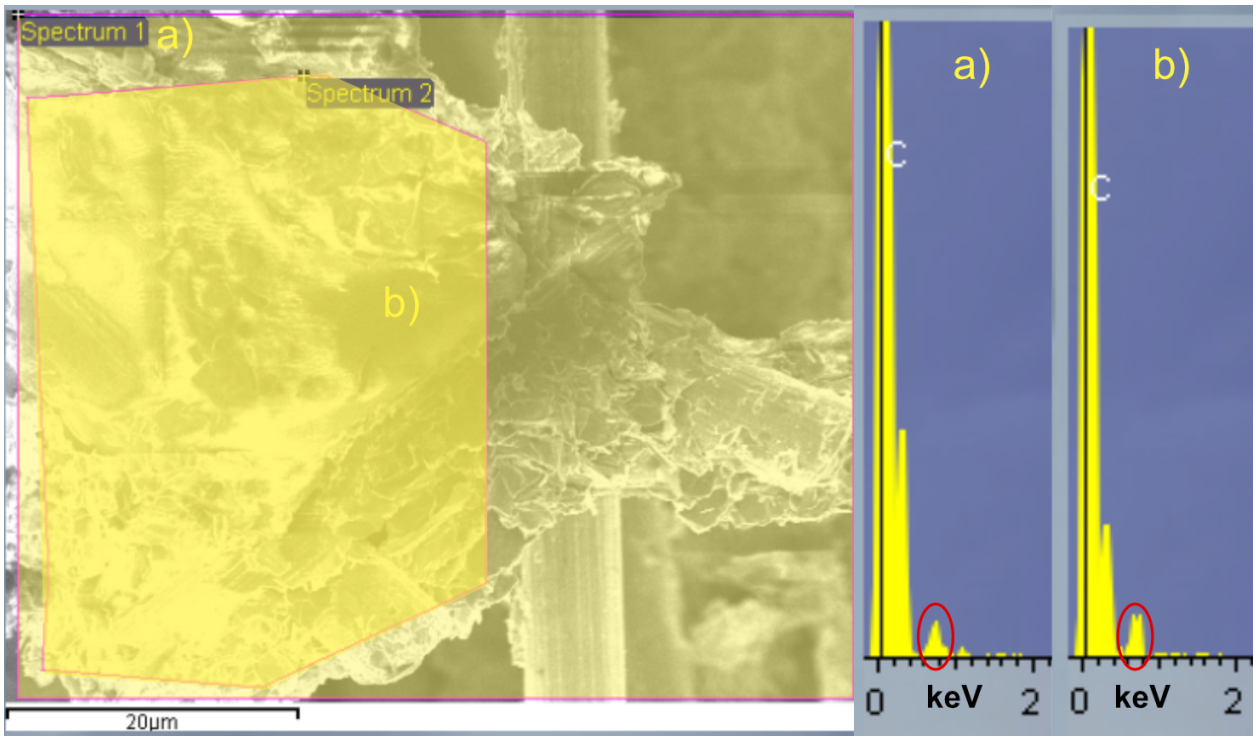

Figure 4.16: SEM image of cross section of sintered SGL 39AA GDL with EDX spectrum spots at 4.85kx magnification

The SEM image of the cross section sintered SGL 39AA GDL shows the fiber binder interface and the presence of binder, as mentioned in the surface EDX analysis due to the preferential accumulation of PTFE between the binder pores, this region was selected for the cross sectional EDX analysis also. However, as stated in the Raman analysis the PTFE distribution across the cross section of the SGL samples showed a very weak intensity peak of flourine. From the above cross section spectrums it is clear that flourine is present accross the crosssection but due to the inability of Raman to characterise its distribution and the weak florine signals from EDX show that PTFE is presence is limited in the cross section and this might be good for diffusion of reactant gases but during higher current densities water management might become a problem leading to flooding of the fuel cell.

4.4 F-H23 SEM and EDX Results

Scanning Electron Microscopy (SEM) was employed to investigate the morphology of the Freudenberg H23 Gas Diffusion Layer (GDL) at various stages of the hydrophobic treatment process. Initially, SEM imaging was conducted on the untreated F-H23 GDL to establish a baseline for the surface and internal morphology. Since the F-H23 is a wet-laid GDL, it has fewer binders and a thick bunch of fibers with relatively much more complicated pore pathways, which may provide resistance for gas transportation.

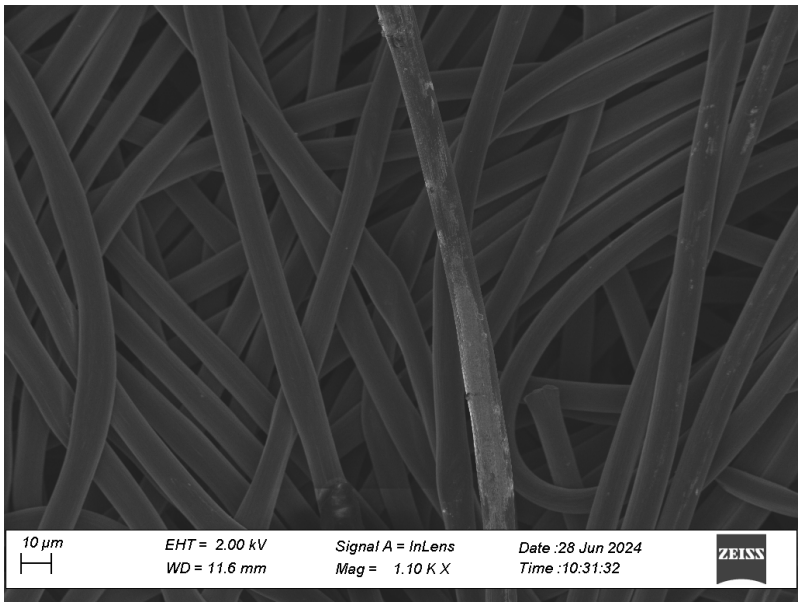

Figure 4.17: Initial morphology of F-H23 without any PTFE showing the thick cluster of fibers at 1.10Kx magnification.

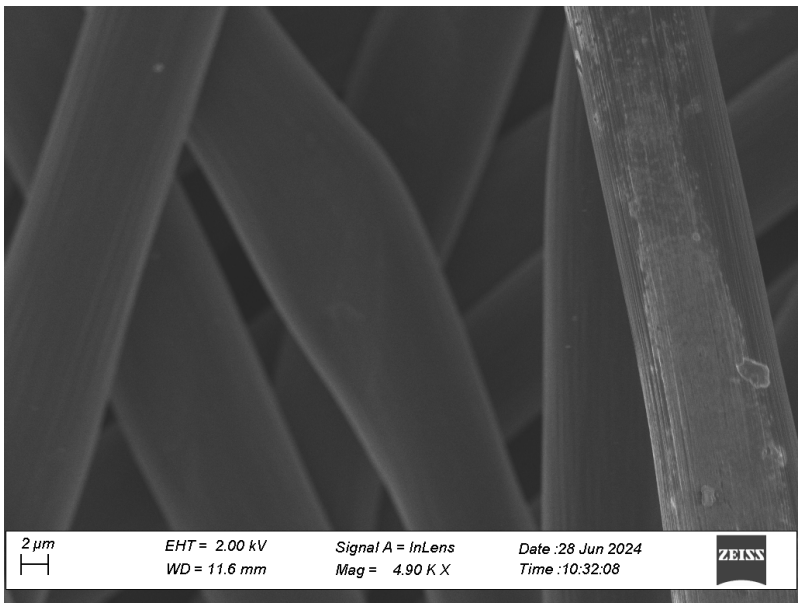

Figure 4.18: Initial morphology of F-H23 without any PTFE at 4.85Kx magnification.

Once the GDLs were dip-coated, it was evident that the PTFE dispersion had preferably adhered around and in between the fibers.

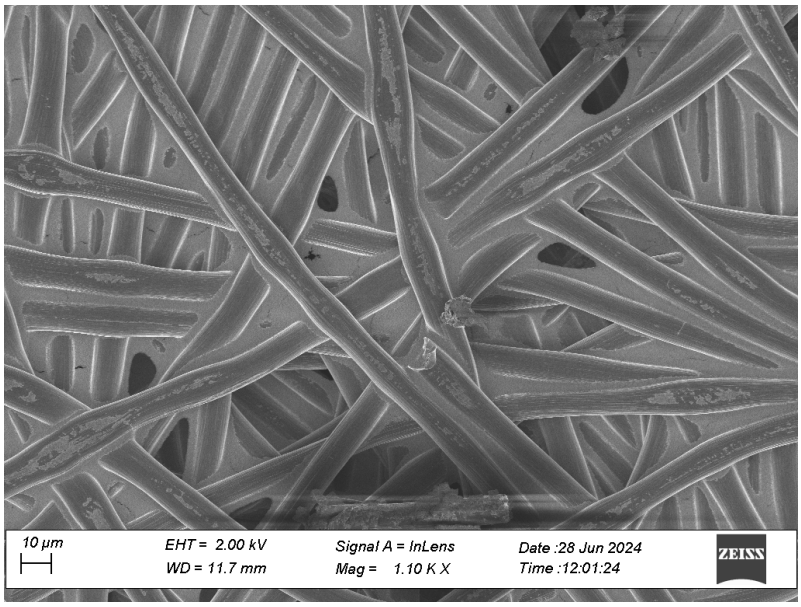

Figure 4.19: Dip-coated F-H23 in which PTFE dispersion can be seen adhered around the fibers at 1.10Kx magnification.

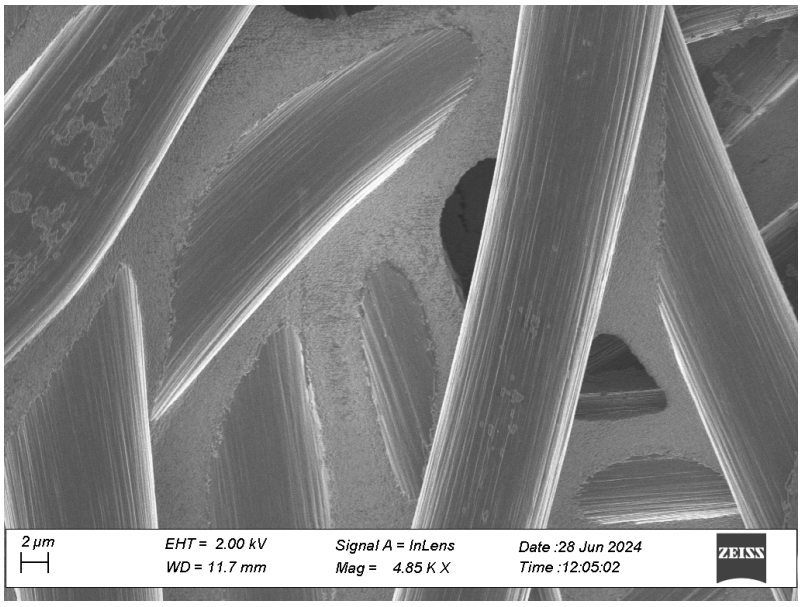

Figure 4.20: Dip-coated F-H23 in which PTFE dispersion can be seen adhered in between the fibers at 4.85Kx magnification.

Once the PTFE dispersion had been sintered, it was observed that the emulsions were removed, and the PTFE particles had melted and adhered around and in between the fibers. Additionally, PTFE agglomerates were noticed in some regions.

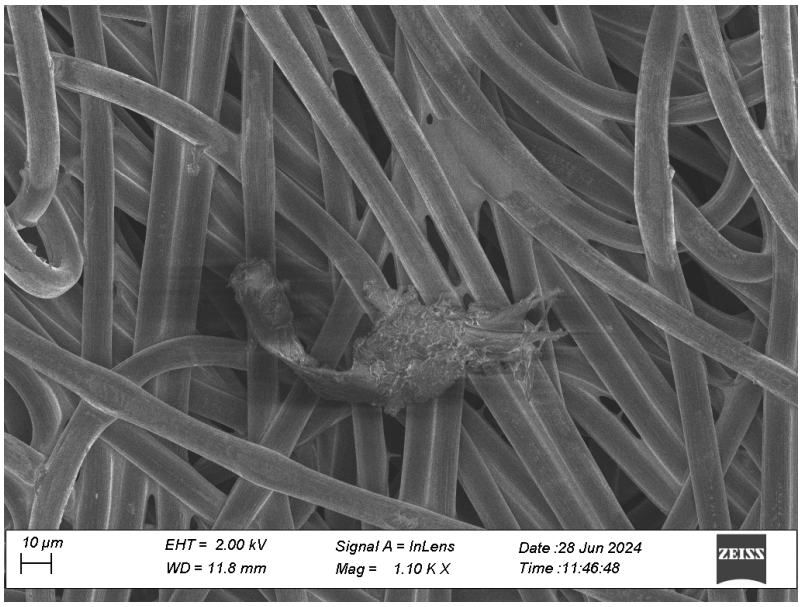

Figure 4.21: Sintered F-H23 in which PTFE particles can be seen adhered around the fibers at 1.10Kx magnification.

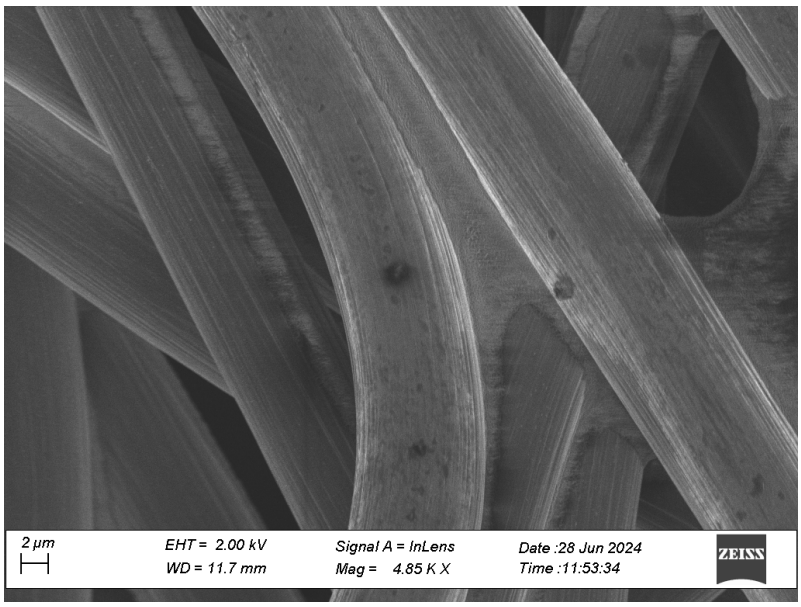

Figure 4.22: Sintered F-H23 in which PTFE particles have formed an agglomerate at 4.85Kx magnification.

The cross section samples were prepared same as the SGL39 AA cross section samples using cryocut method. Figure 4.23 shows the cross section of cryo cut F-H23 GDL it can be seen that the fibers are continous and dense this can also be a contribution to the gas transport resistance results discussed in chapter 4.5

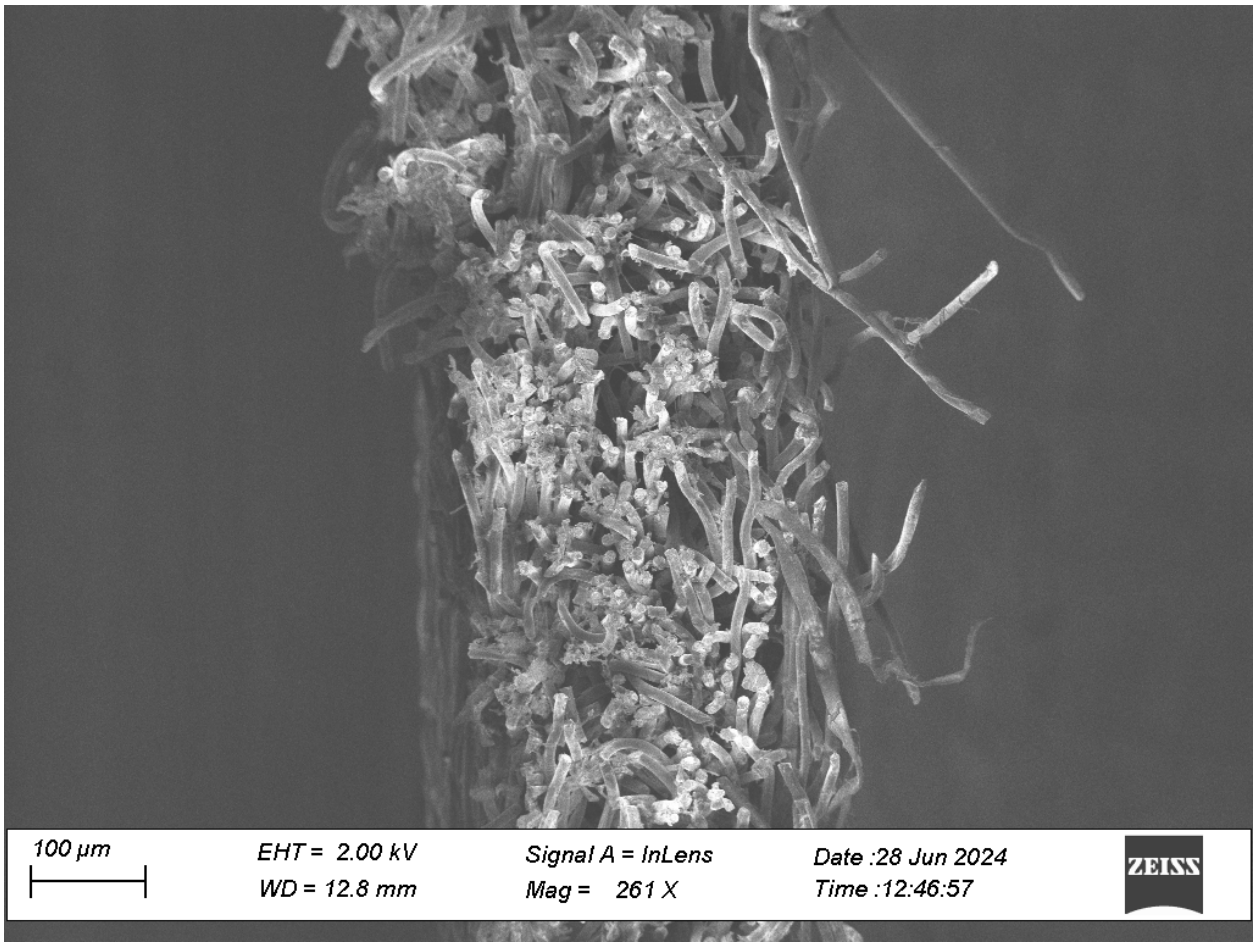

Figure 4.23: Sintered F-H23 in which PTFE particles have formed an agglomerate at 4.85Kx magnification.

4.4.1 EDX Analysis

Energy Dispersive X-ray Spectroscopy (EDX) was performed to verify the presence and distribution of PTFE within and across the F-H23 GDL. In the dip-coated samples, EDX confirmed the presence of fluorine, indicating PTFE adherence primarily between the the fibers and onto the fibres and also accumulations at some points. The sintered and cross sectional samples revealed the same showing the presence of PTFE on and inbetween the fibers.

The following images depict the SEM images that have been focused to obtain the spectrums for all the steps in the hydrophobic treatment process.

Figure 4.24: EDX analysis of plain F-H23.

Figure 4.23 shows the SEM image and the spectrum of the plain F-H23 GDL, it is evident from the large spectrum 4 that there is no presence flourine, which is expected as the intial GDL doesn,t have any flourine.

The EDX analysis was continued with the Dip coated F-H23 samples.

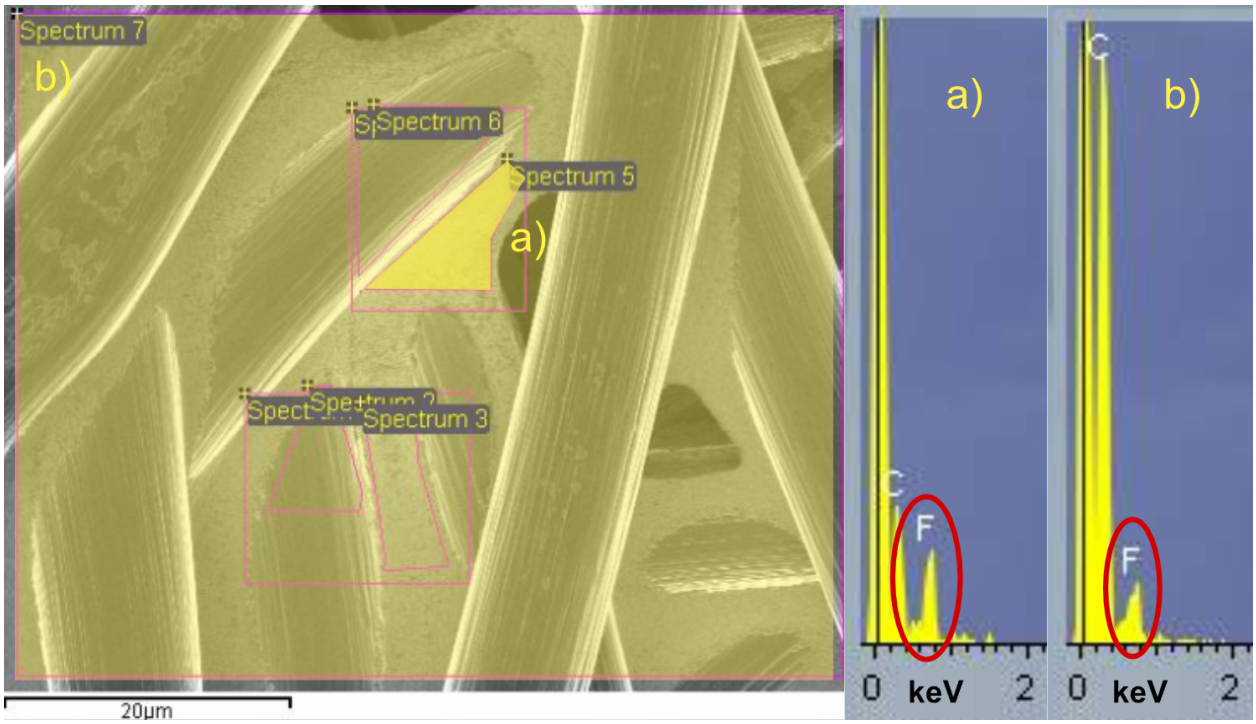

Figure 4.25: EDX Analysis of dip-coated F-H23.

Figure 4.24 shows the SEM image of the dip coated unsinterd F-H23 GDL with the different spectrums that were analysed, this area was chosen for EDX analysis because as earlier mentioned in the SEM part the fibers and the PTFE dispersion have been adhered onto and between the fibers. Spectrum 5 which was done between two fibers evidentally showed the presence of PTFE.

The EDX analysis was further continued with the sintered F-H23 samples.

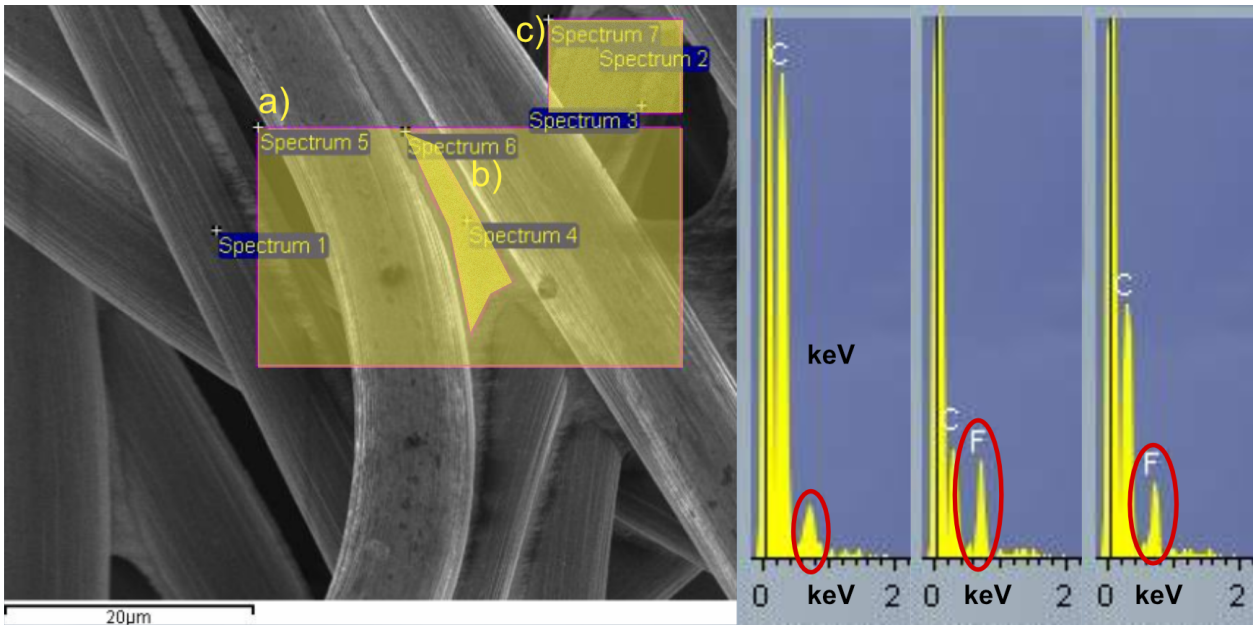

Figure 4.26: SEM image of sintered F-H23 GDL with EDX spectrum spots at 4.85kx magnification

Figure 4.25 shows the SEM image of sintered H23 GDL in which spectrums 6 and 7 revealed the presence of PTFE, unlike the dipcoated GDL PTFE was not found in all the spectrums which is indicated in spectrum 5 were PTFE is not found this shows that PTFE has been sintered and spread out acroos and along the thickness of the GDL. It also can be concluded that the PTFE distribution is not even and homogenous, which is essential for a balance between water management and gas diffusion.

As mentioned earlier from spectrum 5 it is evident that PTFE has been sintered and migrated to different spots. From this it can be concluded that the dip coating method has been good with respect to the F-H23 GDls also.

The EDX analysis was further continued with the cross section of F-H23 sintered samples, these samples were also cry cut like the SGL 39AA samples.

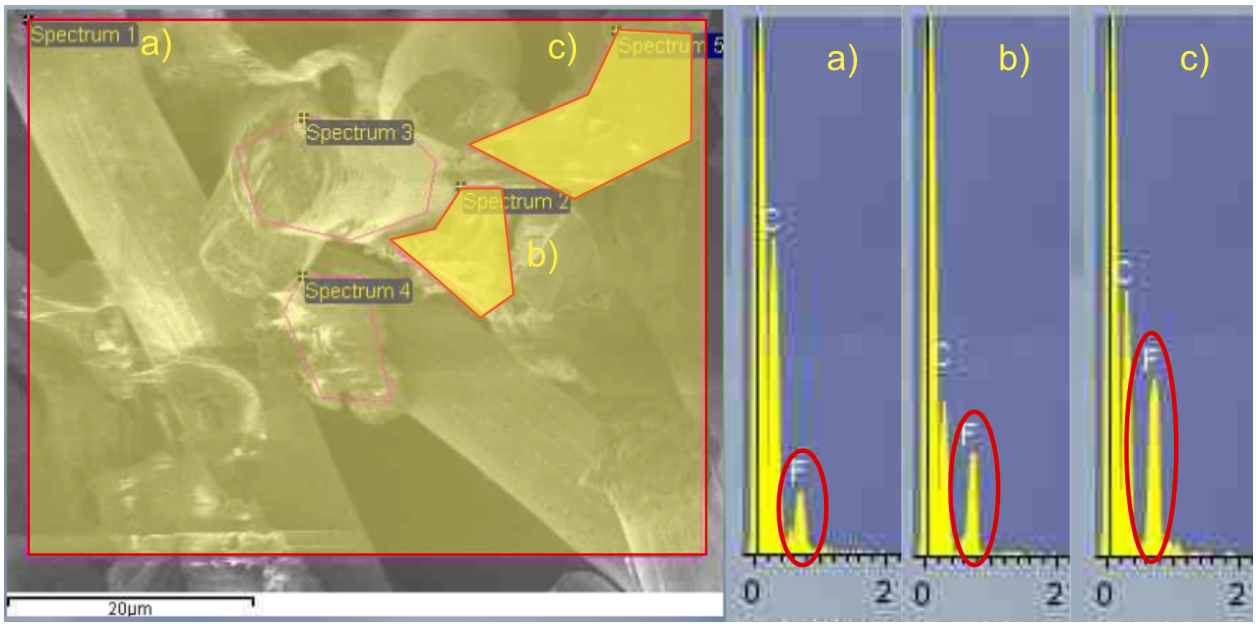

Figure 4.27: SEM image of sintered F-H23 GDL with EDX spectrum spots at 4.85kx magnification

Figure 4.26 shows the SEM image of cross section of sintered F-H23, Unlike the SGL 39AA high intensity peaks of PTFE was found from the spectrums, indicating the presence of PTFE along the thickness of the GDL also.

From spectrum 2 and 5 it is evident that PTFE is evident that PTFE is adhered on and inbetween the fibers, same as the surface analysis.

From the EDX results of F-H23 it can be concluded that F-H23 GDL will perform weel in terms of water management at high current densities.

4.5 Gas Transport Resistance

The transport resistance of different GDLs treated with varying PTFE loadings was measured to assess how these modifications affect the gas transport properties of the GDLs in a PEMFC. The results are summarized in Figure 4.28, which shows the pressure-dependent transport resistance for SGL 39AA and Freudenberg H23 (F-H23) GDLs treated with 5 wt% and 20 wt% PTFE. The 50wt% Gdls were not used in these tests because they didn't perform well in the conditioning phase. This can be due to the influse of higher content of PTFE which may have induced higher ohmic and mass transportation loses.

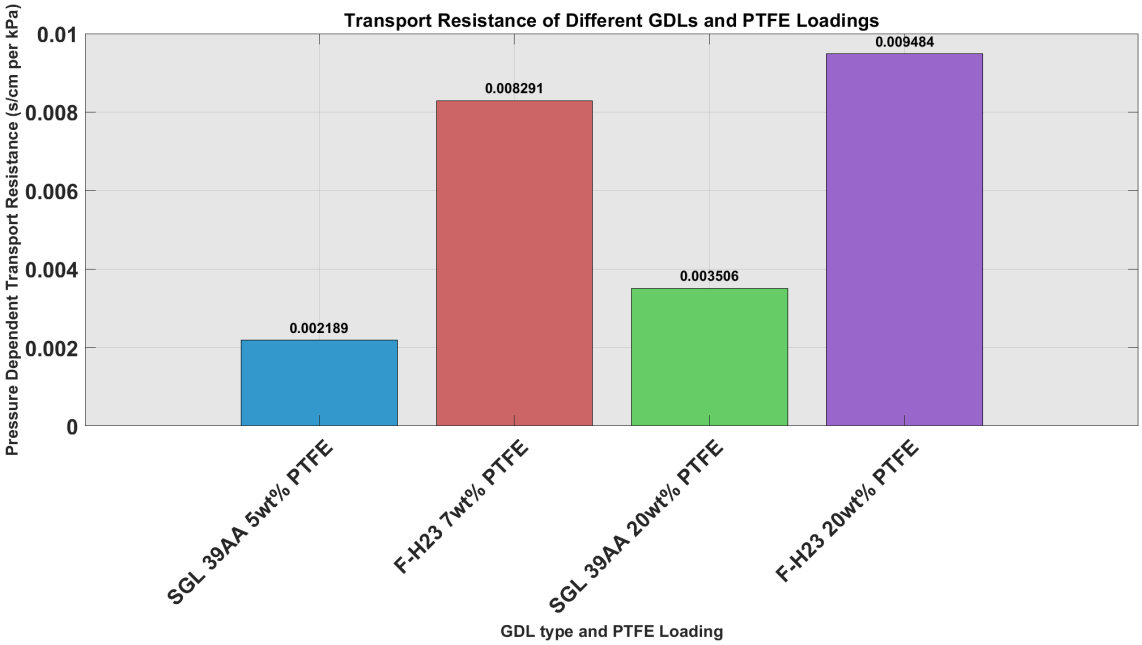

Figure 4.28: Pressure-dependent transport resistance of different GDLs and PTFE loadings.

4.5.1 Transport Resistance Analysis

The results indicate that the transport resistance varies significantly between the different GDLs and PTFE loadings. Specifically, the F-H23 GDL treated with 20 wt% PTFE exhibited the highest transport resistance (0.009484 s/cm per kPa), followed by the F-H23 with 5 wt% PTFE (0.008291 s/cm per kPa). In contrast, the SGL 39AA GDLs showed lower transport resistance values, with the 20 wt% PTFE-treated GDL at 0.003506 s/cm per kPa and the 5 wt% PTFE-treated GDL at 0.002189 s/cm per kPa.

4.5.2 Correlation with SEM and EDX Findings

The higher transport resistance observed in the F-H23 GDLs can be correlated with the SEM and EDX findings, which revealed a more extensive and possibly uneven distribution of PTFE throughout the GDL structure. The SEM images of F-H23 after dip-coating and sintering showed that PTFE adhered extensively around the fibers and filled the pores between them. This extensive coverage, while beneficial for hydrophobicity, can reduce the *effective porosity* of the GDL, which refers to the fraction of pore space that remains accessible for gas transport[25]. As PTFE occupies the pores, the pathways available for oxygen diffusion become narrower or blocked, reducing the overall permeability and gas diffusion capacity of the GDL, thus increasing transport resistance. Moreover, the EDX analysis confirmed the presence of PTFE across the GDL, both on the surface and within the cross-section, with significant PTFE agglomerates forming in certain areas. These agglomerates likely contribute to the reduced permeability and diffusivity of the GDL, resulting in higher transport resistance.

In contrast, the SGL 39AA GDLs demonstrated lower transport resistance, which can be attributed to the less extensive coverage of PTFE observed in the SEM analysis. The SEM images of SGL 39AA showed that while PTFE adhered to the fibers, its distribution was less uniform, with some areas displaying minimal PTFE presence. The EDX results supported this, showing weaker fluorine signals, especially in the cross-sectional analysis, indicating that PTFE did not penetrate deeply into the GDL. This more limited coverage likely preserved more of the GDL's inherent porosity, allowing for better gas transport and consequently lower transport resistance.

4.5.3 Impact of PTFE Loading on GDL Performance

The results also highlight the impact of PTFE loading on transport resistance. For both GDL types, increasing the PTFE content from 5 wt% to 20 wt% led to an increase in transport resistance. This trend suggests that while higher PTFE loading improves hydrophobicity and prevents flooding, it can also hinder gas transport by clogging the pores within the GDL. This trade-off between hydrophobicity and gas transport efficiency must be carefully managed to optimize the performance of PEMFCs.

4.5.4 Raman Spectroscopy Correlation

Raman spectroscopy provided further insights into the PTFE distribution within the GDLs. For the SGL 39AA, Raman mapping showed that PTFE was primarily located in the pores between the fibers and binders, rather than being uniformly distributed. This uneven distribution corresponds with the lower transport resistance observed in the SGL 39AA GDLs, as the less dense PTFE coverage allowed for more efficient gas diffusion pathways.
On the other hand, the F-H23 GDLs exhibited a more thorough PTFE coverage, as confirmed by Raman spectroscopy, which detected PTFE across both the surface and through the cross-section of the GDL. The extensive PTFE presence, especially in the form of agglomerates, is likely a significant factor contributing to the higher transport resistance observed in the F-H23 GDLs.

5

Conclusion and Future Work

In conclusion, this study provides a comprehensive analysis of the hydrophobic treatment of Gas Diffusion Layers (GDLs) using polytetrafluoroethylene (PTFE) to enhance the performance and longevity of Proton Exchange Membrane Fuel Cells (PEMFCs). By systematically investigating both dry-laid (SGL 39AA) and wet-laid (Freudenberg H23) GDLs, the research highlights the critical role of PTFE distribution and concentration in optimizing water management and gas transport properties within the GDLs.

The findings demonstrate that proper PTFE content is crucial in minimizing oxygen transport resistance, a key factor in ensuring efficient fuel cell operation. Achieving the right balance of PTFE concentration proved to be particularly challenging, as it required careful calibration to ensure that the GDLs became sufficiently hydrophobic without excessively blocking pores and hindering oxygen diffusion. This study found that while increasing PTFE content enhances the hydrophobicity of the GDLs, it also introduces potential drawbacks, such as pore blockage and increased transport resistance, which can negatively impact gas diffusion.

The hydrophobic treatment process, especially in achieving the correct PTFE wt%, was critical to the success of the GDL modification. Through repeated experimentation, it became clear that optimizing PTFE concentration was not just about enhancing water-repellency but also about preserving the delicate balance between hydrophobicity and the GDL's inherent gas transport capabilities. This balance is essential for maintaining the overall efficiency of the PEMFC.

The research also revealed that the microstructure of the GDL, influenced by its manufacturing process (dry-laid versus wet-laid), plays a significant role in determining the effectiveness of PTFE treatment. The dry-laid SGL 39AA, with its more uniform pore structure accross the binders, exhibited better control over PTFE distribution and lower oxygen transport resistance compared to the more complex and variable pore structure of the wet-laid Freudenberg H23, this is visible form the cross section SEM image of F-H23, which shows a thick cluster of fibers. This indicates that the selection of GDL material and the optimization of PTFE treatment must be tailored to the specific demands of the fuel cell application. But the unavailability of PTFE in the cross sections of SGL 39AA GDLs could be a draw back at higher current densities were water management is crucial. In that case the F-H23 GDLs may perform well at high current densities.

Advanced characterization techniques, including Scanning Electron Microscopy (SEM), Energy Dispersive X-ray Spectroscopy (EDX), and Raman Spectroscopy, were employed to provide a detailed understanding of the PTFE distribution across the GDLs. These analyses confirmed the presence of PTFE in critical regions of the GDL, correlating the distribution patterns with the observed transport properties. The study's in-situ and ex-situ performance evaluations, including contact angle measurements and limiting current density assessments, further validated the impact of PTFE loading on GDL functionality.

Overall, this research advances the understanding of how hydrophobic treatments affect GDL performance in PEMFCs, offering valuable insights for the development of high-performance fuel cells. By emphasizing the importance of uniform PTFE distribution, the careful selection of PTFE concentration, and the challenges associated with optimizing the hydrophobic treatment, this study lays the groundwork for future innovations aimed at optimizing GDL design and treatment processes. These findings are expected to contribute significantly to the ongoing efforts to improve the efficiency, durability, and commercial viability of PEMFCs.

Future Work

In future work, several aspects of the hydrophobic treatment process and GDL characterization should be further explored to enhance the understanding and performance of PEMFCs:

- **Dip Coating Process**: It is crucial to investigate how the dipping time affects the PTFE content in the GDL. Although the PTFE dispersion was diluted from 60 wt% to the desired concentration, the study found that dipping the GDLs for more than 15 to 30 seconds led to a higher PTFE wt%. This aspect needs to be systematically studied to optimize the dipping process and improve the hydrophobic treatment method.

- **Raman Spectroscopy**: Future research should focus on characterizing the PTFE content in the cross-section of SGL 39AA, as this proved challenging in the current study. Additionally, Raman mapping should be conducted over a larger area to better characterize the distribution of PTFE and identify any inconsistencies.

- **In-Situ Measurements**: The in-situ measurements used to determine transport resistance should be repeated multiple times to ensure optimal accuracy and reliability in the results. Repeating these measurements will help to confirm the trends observed and provide a more robust set of conclusions.

- **Bulk Properties Testing**: It is important to test the bulk properties of the GDL with varying PTFE content, as the PTFE concentration can alter mechanical, thermal, and electrical properties. Understanding these changes is essential for optimizing the GDL for different fuel cell applications.

- **Microporous Layer (MPL) Coating**: Future studies should also consider coating and characterizing the Microporous Layer (MPL) on the GDL. Investigating its influence on transport resistance and overall fuel cell performance could provide valuable insights for further improvements in PEMFC efficiency.

This future work will build on the findings of this study, driving continued advancements in the development of high-performance fuel cells.

Bibliography

[1] Xiao-Zi Yuan and Haijiang Wang. PEM Fuel Cell Fundamentals. Technical report.

[2] San Ping Jiang and Qingfeng Li. Introduction to Fuel Cells Electrochemistry and Materials Introduction to Fuel Cells Introduction to Fuel Cells. Technical report.

[3] https://en.wikipedia.org/wiki/Energy-dispersive_X-ray_spectroscopy.

[4] Grigoria Athanasaki, Arunkumar Jayakumar, and A. M. Kannan. Gas diffusion layers for PEM fuel cells: Materials, properties and manufacturing – A review. *International Journal of Hydrogen Energy*, 48(6):2294–2313, 1 2023.

[5] Linda Carrette, K. Andreas Friedrich, and Ulrich Stimming. Fuel Cells: Principles, Types, Fuels, and Applications. *ChemPhysChem*, 1(4):162–193, 12 2000.

[6] Asif Jamil, Sikander Rafiq, Tanveer Iqbal, Hafiza Aroosa Aslam Khan, Haris Mahmood Khan, Babar Azeem, M. Z. Mustafa, and Abdulkader S. Hanbazazah. Current status and future perspectives of proton exchange membranes for hydrogen fuel cells. *Chemosphere*, 303, 9 2022.

[7] Final Report Advanced Cathode Catalysts and Supports for PEM Fuel Cells Key Vendor for Stack Testing: GM Fuel Cell Activities. Technical report.

[8] Paul C. Okonkwo and Clement Otor. A review of gas diffusion layer properties and water management in proton exchange membrane fuel cell system, 3 2021.

[9] Daniel R. Baker, Christian Wieser, Kenneth C. Neyerlin, and Michael W. Murphy. The Use of Limiting Current to Determine Transport Resistance in PEM Fuel Cells. *ECS Transactions*, 3(1):989–999, 10 2006.

[10] Daniel R. Baker, David A. Caulk, Kenneth C. Neyerlin, and Michael W. Murphy. Measurement of Oxygen Transport Resistance in PEM Fuel Cells by Limiting Current Methods. *Journal of The Electrochemical Society*, 156(9):B991, 2009.

[11] Noriko Hikosaka Behling. Fuel Cells and the Challenges Ahead. In *Fuel Cells*, pages 7–36. Elsevier, 2013.

[12] Christoph Simon, Dena Kartouzian, David Müller, Florian Wilhelm, and Hubert A. Gasteiger. Impact of Microporous Layer Pore Properties on Liquid Water Transport in PEM Fuel Cells: Carbon Black Type and Perforation. *Journal of The Electrochemical Society*, 164(14):F1697–F1711, 2017.

[13] Mark Mathias, Joerg Roth, Jerry Fleming, and Werner Lehnert. Chapter 46 Diffusion media materials and characterisation. Technical report.

[14] Freudenberg Performance Materials. Wetlaid Nonwovens, 2024.

[15] PerkinElmer Inc. Thermogravimetric Analysis (TGA) TGA 8000 TGA 4000 STA 6000 / STA 8000 The Thermogravimetric Instrument Family. Technical report.

[16] Babu V Bassa and Rao M Uppu. Modification of the Basic Dilution Equation for the Programming of Serial Dilutions. Technical report.

[17] Chan Lim and C. Y. Wang. Effects of hydrophobic polymer content in GDL on power performance of a PEM fuel cell. *Electrochimica Acta*, 49(24):4149–4156, 9 2004.

[18] A. J. Mendoza, M. A. Hickner, J. Morgan, K. Rutter, and C. Legzdins. Raman spectroscopic mapping of the carbon and PTFE distribution in gas diffusion layers. *Fuel Cells*, 11(2):248–254, 4 2011.

[19] Mehdi Alipour and A. Sakhaee-Pour. Application of Young-Laplace with size-dependent contact angle and interfacial tension in shale. *Geoenergy Science and Engineering*, 231:212447, 12 2023.

[20] Md Azimur Rahman, Felipe Mojica, Mrittunjoy Sarker, and Po Ya Abel Chuang. Development of 1-D multiphysics PEMFC model with dry limiting current experimental validation. *Electrochimica Acta*, 320, 10 2019.

[21] Colleen Spiegel. *PEM Fuel Cell Modeling and Simulation Using Matlab*. Elsevier, 2008.

[22] Veeresh Patil, P. V. Reshmi, S. Prajna, Yashaswi, Yashaswini, D. Haleshappa, A. Jayarama, and Richard Pinto. Degradation mechanisms in PEM fuel cells: A brief review. *Materials Today: Proceedings*, 2023.

[23] Nobuaki Nonoyama, Shinobu Okazaki, Adam Z. Weber, Yoshihiro Ikogi, and Toshihiko Yoshida. Analysis of Oxygen-Transport Diffusion Resistance in Proton-Exchange-Membrane Fuel Cells. *Journal of The Electrochemical Society*, 158(4):B416, 2011.

[24] Christoph Simon, Frédéric Hasché, David Müller, and Hubert A. Gasteiger. Influence of the Gas Diffusion Layer Compression on the Oxygen Mass Transport in PEM Fuel Cells. *ECS Transactions*, 69(17):1293–1302, 9 2015.

[25] Yuan Gao, Angel Montana, and Fengxiang Chen. Evaluation of porosity and thickness on effective diffusivity in gas diffusion layer. *Journal of Power Sources*, 342:252–265, 2 2017.

A

Appendix 1

The MATLAB code used for the interpretation of the Gas transport results has been mentioned in this section it would be helpful to understand the step by step calculation of the results:

```
clc;
clear all;

%% 2 bar pressure
% Load data from Excel file
[~, ~, raw] = xlsread('F:\OTR results\Excel files\SGL 39AA 5wt.xlsx');

% Define a function to convert and clean data
cleanData = @(col) cell2mat(cellfun(@(x) str2double(x), raw(2:end, col), 'UniformOutput', false));

% Extract and clean the data for each set
current_density_4 = cleanData(1);
voltage_4 = cleanData(2);

current_density_2 = cleanData(4);
voltage_2 = cleanData(5);

current_density_1 = cleanData(7);
voltage_1 = cleanData(8);

current_density_0_5 = cleanData(10);
voltage_0_5 = cleanData(11);

% Function to remove NaN values from the data
removeNaNs = @(x, y) deal(x(~isnan(x) & ~isnan(y)), y(~isnan(x) & ~isnan(y)));

% Remove NaN values from each set
[current_density_4, voltage_4] = removeNaNs(current_density_4, voltage_4);
[current_density_2, voltage_2] = removeNaNs(current_density_2, voltage_2);
[current_density_1, voltage_1] = removeNaNs(current_density_1, voltage_1);
[current_density_0_5, voltage_0_5] = removeNaNs(current_density_0_5, voltage_0_5);

% Plot the data
figure;
hold on;
plot(current_density_4, voltage_4, '-o', 'DisplayName', '4% 3 bar');
plot(current_density_2, voltage_2, '-*', 'DisplayName', '2% 3 bar');
plot(current_density_1, voltage_1, '-x', 'DisplayName', '1% 3 bar');
plot(current_density_0_5, voltage_0_5, '-s', 'DisplayName', '0.5% 3 bar');

% Customize the plot
xlabel('Current Density');
ylabel('Cell Voltage Max');
title('Current Density vs Cell Voltage Max');
legend show;
grid on;
hold off;

%% 1 bar pressure
% Load data from Excel file
[~, ~, raw] = xlsread('F:\OTR results\Excel files\SGL 39AA 5wt.xlsx');
```

```
% Define a function to convert and clean data
cleanData = @(col) cell2mat(cellfun(@(x) str2double(x), raw(2:end, col), 'UniformOutput', false));

% Extract and clean the data for each set
current_density_4 = cleanData(13);
voltage_4 = cleanData(14);

current_density_2 = cleanData(16);
voltage_2 = cleanData(17);

current_density_1 = cleanData(19);
voltage_1 = cleanData(20);

current_density_0_5 = cleanData(22);
voltage_0_5 = cleanData(23);

% Function to remove NaN values from the data
removeNaNs = @(x, y) deal(x(~isnan(x) & ~isnan(y)), y(~isnan(x) & ~isnan(y)));

% Remove NaN values from each set
[current_density_4, voltage_4] = removeNaNs(current_density_4, voltage_4);
[current_density_2, voltage_2] = removeNaNs(current_density_2, voltage_2);
[current_density_1, voltage_1] = removeNaNs(current_density_1, voltage_1);
[current_density_0_5, voltage_0_5] = removeNaNs(current_density_0_5, voltage_0_5);

% Plot the data
figure;
hold on;
plot(current_density_4, voltage_4, '-o', 'DisplayName', '4% 2 bar');
plot(current_density_2, voltage_2, '-*', 'DisplayName', '2% 2 bar');
plot(current_density_1, voltage_1, '-x', 'DisplayName', '1% 2 bar');
plot(current_density_0_5, voltage_0_5, '-s', 'DisplayName', '0.5% 2 bar');

% Customize the plot
xlabel('Current Density');
ylabel('Cell Voltage Max');
title('Current Density vs Cell Voltage Max');
legend show;
grid on;
hold off;

%% 1.5 bar pressure
% Load data from Excel file
[~, ~, raw] = xlsread('F:\OTR results\Excel files\SGL 39AA 5wt.xlsx');

% Define a function to convert and clean data
cleanData = @(col) cell2mat(cellfun(@(x) str2double(x), raw(2:end, col), 'UniformOutput', false));

% Extract and clean the data for each set
current_density_4 = cleanData(25);
voltage_4 = cleanData(26);

current_density_2 = cleanData(28);
voltage_2 = cleanData(29);

current_density_1 = cleanData(31);
voltage_1 = cleanData(32);

current_density_0_5 = cleanData(34);
voltage_0_5 = cleanData(35);

% Function to remove NaN values from the data
removeNaNs = @(x, y) deal(x(~isnan(x) & ~isnan(y)), y(~isnan(x) & ~isnan(y)));

% Remove NaN values from each set
[current_density_4, voltage_4] = removeNaNs(current_density_4, voltage_4);
[current_density_2, voltage_2] = removeNaNs(current_density_2, voltage_2);
[current_density_1, voltage_1] = removeNaNs(current_density_1, voltage_1);
[current_density_0_5, voltage_0_5] = removeNaNs(current_density_0_5, voltage_0_5);
```

```
% Plot the data
figure;
hold on;
plot(current_density_4, voltage_4, '-o', 'DisplayName', '4% 1.5 bar');
plot(current_density_2, voltage_2, '-*', 'DisplayName', '2% 1.5 bar');
plot(current_density_1, voltage_1, '-x', 'DisplayName', '1% 1.5 bar');
plot(current_density_0_5, voltage_0_5, '-s', 'DisplayName', '0.5% 1.5 bar');

% Customize the plot
xlabel('Current Density');
ylabel('Cell Voltage Max');
title('Current Density vs Cell Voltage Max');
legend show;
grid on;
hold off;

%% ilim vs O2 conc
% Data
O2_conc = [0.04, 0.02, 0.01, 0.005]; % Updated to make 0.04 (4% O2 concentration) the first value
Pressure = [300000, 200000, 150000]; % Pressure in Pa

% ilim values for each combination of O2 conc and Pressure
% Convert ilim_4_percent from A/cm² to A/m² by multiplying by 10,000
ilim_4_percent = [2.02597; 1.77621; 1.58235] * 10000;

% ilim values for 0.04 O2 (converted from A/cm² to A/m²) and other O2 concs
ilim = [
    ilim_4_percent(1), 11202.5, 5618.46, 2676.14; % For 300 KPa
    ilim_4_percent(2), 9267.02, 4506.68, 2077.96; % For 200 KPa
    ilim_4_percent(3), 8095.72, 3875.62, 1763.2   % For 150 KPa
];

% Debugging: Print sizes
disp(['Size of O2_conc: ', mat2str(size(O2_conc))]);
disp(['Size of Pressure: ', mat2str(size(Pressure))]);
disp(['Size of ilim: ', mat2str(size(ilim))]);

% Plot initial data
figure; % Create a new figure
hold on; % Hold on to add multiple plots
colors = ['r', 'g', 'b']; % Different colors for different pressures

for i = 1:length(Pressure)
    plot(O2_conc, ilim(i, :), '-o', 'DisplayName', [num2str(Pressure(i)) ' Pa'], 'Color', colors(i));
end

xlabel('Dry Mole Fraction Oxygen');
ylabel('Limiting Current (ilim)');
title('ilim vs O2 Concentration at Different Pressures');
legend('show'); % Show legend
grid on; % Add grid
hold off; % Release hold

%% Slope of the graph and R^2 calculation
% Initialize array to store slopes and R^2 values
slopes = zeros(length(Pressure), 1);
R2_values = zeros(length(Pressure), 1);

% Create a new figure for slope and R^2 plots
figure;
hold on; % Hold on to add multiple plots

for i = 1:length(Pressure)
    % Fit a linear polynomial (1st degree) to the data
    p = polyfit(O2_conc, ilim(i, :), 1); % 1 means linear fit

    % Store the slope (the first coefficient of the polynomial)
    slopes(i) = p(1);

    % Calculate the fitted values
```

```
    yfit = polyval(p, O2_conc);

    % Calculate R^2
    ymean = mean(ilim(i, :));
    SS_tot = sum((ilim(i, :) - ymean).^2);
    SS_res = sum((ilim(i, :) - yfit).^2);
    R2_values(i) = 1 - (SS_res / SS_tot);  % Correct indexing with parentheses

    % Display the slope and R^2
    fprintf('Slope for %d Pa pressure: %f\n', Pressure(i), slopes(i));
    fprintf('R^2 for %d Pa pressure: %f\n', Pressure(i), R2_values(i));  % Correct indexing with parentheses

    % Plot the original data points
    plot(O2_conc, ilim(i, :), 'o', 'DisplayName', sprintf('%d Pa data', Pressure(i)), 'Color', colors(i));

    % Plot the fitted line
    plot(O2_conc, yfit, '-', 'DisplayName', sprintf('%d Pa fit (R^2 = %.4f)', Pressure(i), R2_values(i)), 'Color', colors

    % Extend the line beyond the data range to see where it intersects the axes
    extended_x = [0, O2_conc, max(O2_conc) * 1.5]; % Extend x to 1.5 times the max O2 concentration
    extended_y = polyval(p, extended_x); % Calculate the corresponding y values
    plot(extended_x, extended_y, '--', 'Color', colors(i), 'HandleVisibility', 'off'); % Dashed line for extended fit
end

% Add labels and legend
xlabel('Dry Mole Fraction Oxygen');
ylabel('Limiting Current (ilim)');
title('Linear Fit with Slopes and R^2 Values at Different Pressures');
legend('show');
grid on; % Add grid

% Set the x-axis and y-axis to start from the origin (0, 0)
xlim([0, max(extended_x)]); % Adjust x-axis limits to include a little margin
ylim([0, max(ilim(:)) * 1.1]); % Adjust y-axis limits to include a little margin

% Display the final plot
hold off;
%% Constants
F = 96485.485; % Faraday's constant in C/mol
R = 8.314; % Universal gas constant in J/mol·K
T = 343.15; % Temperature in Kelvin (70°C)
p_W = 31824; % Partial pressure of water in Pa (converted from 31.824 kPa)

%% Slope values from the previous calculation
% slopes = [slope_300kPa, slope_200kPa, slope_150kPa]; % Already calculated in your code

% Pressure values
Pressure = [300000, 200000, 150000]; % in Pa

%% Calculate Transport Resistance (R_T) for each pressure
Rt = zeros(length(Pressure), 1);

for i = 1:length(Pressure)
    % Calculate the pressure difference
    delta_p = Pressure(i) - p_W;

    % Calculate transport resistance using the given formula
    Rt(i) = (4 * F * delta_p) / (slopes(i) * R * T)/100;

    % Display the transport resistance
    fprintf('Transport resistance for %d Pa pressure: %f s/cm\n', Pressure(i), Rt(i));
end

%% Convert Pressure from Pa to kPa for plotting
Pressure_kPa = Pressure / 1000; % Convert Pa to kPa

%% Perform a linear fit on the calculated transport resistance vs. pressure in kPa
p_fit = polyfit(Pressure_kPa, Rt, 1); % p_fit(1) is the slope, p_fit(2) is the intercept

% Generate fitted values for plotting
```

```
fitted_Rt = polyval(p_fit, Pressure_kPa);

% Display the slope of the linear fit
fprintf('Slope of the linear fit (R_T vs Pressure in kPa): %f s/cm per kPa\n', p_fit(1));
%% Given Pressure values in kPa and corresponding Rt values
Pressure_kPa = [300, 200, 150];  % Pressures in kPa (converted from Pa)
Rt = [0.727210, 0.509370, 0.398677]; % Your updated Rt values in s/cm

% Fit a linear model to the data
p_fit = polyfit(Pressure_kPa, Rt, 1); % Perform linear regression

% Calculate the fitted values
fitted_Rt = polyval(p_fit, Pressure_kPa);

% Calculate R^2 correctly
SS_res = sum((Rt - fitted_Rt).^2); % Residual sum of squares
SS_tot = sum((Rt - mean(Rt)).^2); % Total sum of squares
R2 = 1 - (SS_res / SS_tot); % Coefficient of determination

% Display the slope of the linear fit and R^2
fprintf('Slope of the linear fit (R_T vs Pressure in kPa): %f s/cm per kPa\n', p_fit(1));
fprintf('R^2 of the linear fit (R_T vs Pressure in kPa): %f\n', R2);

% Plot the data points and the fitted line
figure;
plot(Pressure_kPa, Rt, 'bo', 'DisplayName', 'Calculated Rt values'); % Data points
hold on;
plot(Pressure_kPa, fitted_Rt, 'r-', 'DisplayName', 'Linear fit'); % Fitted line

% Add legend and R^2 annotation
legend('Location', 'northwest');
text(0.1, 0.9, sprintf('R^2 = %.4f', R2), 'Units', 'normalized', 'FontSize', 12, 'BackgroundColor', 'white');

% Add labels and title
xlabel('Pressure (kPa)');
ylabel('Transport Resistance (s/cm)');
title('Transport Resistance vs. Pressure (kPa)');
grid on;
xlim([0, max(Pressure_kPa)]);
ylim([0, max(Rt) * 1.1]); % Adjust y-axis to start from 0 and provide a bit of margin at the top
hold off;


%% Plot the Transport Resistance vs Pressure (in kPa) with linear fit
figure;
plot(Pressure_kPa, Rt, 'bo', 'DisplayName', 'Calculated Rt values'); % Data points
hold on;
plot(Pressure_kPa, fitted_Rt, 'r-', 'DisplayName', sprintf('Linear fit: Rt = %.4e * P + %.4f', p_fit(1), p_fit(2))); % Fi
xlabel('Pressure (kPa)');
ylabel('Transport Resistance (s/m)');
title('Transport Resistance vs. Pressure (kPa)');
legend('Location', 'northwest');
grid on;
xlim([0, max(Pressure_kPa)]);
ylim([0, max(Rt) * 1.1]); % Adjust y-axis to start from 0 and provide a bit of margin at the top
hold off;
%% Define the new ilim values for 4% O2 concentration
O2_conc_4_percent = 0.04; % 4% O2 concentration as a decimal
ilim_4_percent = [
    2.02597; % For 2 bar
    1.77621; % For 1 bar
    1.58235;  % For 0.5 bar
];

% Update the O2 concentration array to include 4%
O2_conc = [0.02, 0.01, 0.005, O2_conc_4_percent]; % Adding 4% to the existing O2 concentrations

% Update the ilim array to include the new values for 4%
ilim = [
    5.0563e3, 2.71058e3, 1.39836e3, ilim_4_percent(1); % For 300 kPa (2 bar)
```

```
    6.77254e3, 3.47162e3, 1.75068e3, ilim_4_percent(2); % For 200 kPa (1 bar)
    6.2464e3, 3.11302e3, 1.48134e3, ilim_4_percent(3)  % For 150 kPa (0.5 bar)
];

% Convert ilim from A/m² to A/cm² for existing values (excluding 4% which is already in A/cm²)
ilim_cm2 = ilim; % Keep the existing values as they are
ilim_cm2(:, 1:end-1) = ilim(:, 1:end-1) / 10000; % Convert only the old values from A/m² to A/cm²

% Define colors for different pressures
pressure_colors = {'r', 'b', 'k'}; % Red for 300 kPa, Blue for 200 kPa, Black for 150 kPa

% Create the plot
figure;
hold on;

% Plot each pressure level with different colors and markers representing O2 concentrations
for i = 1:length(Pressure)
    for j = 1:length(O2_conc)
        plot(ilim_cm2(i, j), Rt(i), 's', 'MarkerSize', 8, ...
             'MarkerFaceColor', pressure_colors{i}, 'MarkerEdgeColor', pressure_colors{i}, ...
             'DisplayName', sprintf('Pressure: %d kPa, O2 Conc: %.1f%%', Pressure(i)/1000, O2_conc(j) * 100));
    end
end

% Customize the plot to match the example
xlabel('Limiting current density / A/cm^2');
ylabel('Transport resistance / S/cm');
title('Dry plateau');
legend('Location', 'northeastoutside');
grid on;
xlim([min(ilim_cm2(:))-0.1, max(ilim_cm2(:))+0.1]);
ylim([min(Rt)-0.1, max(Rt)+0.1]);
hold off;
```

The above code was used for calculating the results for SGL 39AA 5wt% PTFE GDL. The same code was used for calculating the results for the other three GDLs.